The Thesis Committee for Jieyi Zhu
Certifies that this is the approved version of the following thesis:

Utp14 recruits and activates the RNA helicase Dhr1 to undock U3 snoRNA from the pre-ribosome

APPROVED BY
SUPERVISING COMMITTEE:

Supervisor:

Arlen Johnson

Scott Stevens

Utp14 recruits and activates the RNA helicase Dhr1 to undock U3 snoRNA from the pre-ribosome

by

Jieyi Zhu, B. AGRICULTURE; M. AGRICULTURE

Thesis

Presented to the Faculty of the Graduate School of

The University of Texas at Austin

in Partial Fulfillment

of the Requirements

for the Degree of

Master of Arts

The University of Texas at Austin

May 2016

Acknowledgements

I would like to thank my advisor and mentor Dr. Arlen Johnson for giving me the opportunity to join his lab and study this wonderful project- ribosome biogenesis. He has continuously provided me with expert wisdom throughout my research and showed full support and encouragement for me through the ups and downs of my graduate career. I would also like to thank the other members of our lab that I have been fortunate to work with. Dr. Richa Sardana, who is a former member of our lab, gave me great guidance in the beginning of my graduate study. My lab mates Stephanie Patchett, Dr. Zhaohui Huang, Dr. Sharmishtha Musalgaonkar, Margarida Anjos, and Jeffrey Recchia-Rife, have all been consistently supportive and I thank them for making my life in Arlen's lab so enjoyable. I would also like to thank Dr. Scott Stevens for providing his valuable comments on my research, and spending his precious time in reading and commenting on this thesis. I would also like to thank our collaborator Dr. Carl Correll and his former student Dr. Xin Liu. It was wonderful to working with you guys. Finally, I would like to show my deepest appreciation to my family members who have shown ceaseless support for my graduate study here. Especially, I thank my husband Shanzhong Gong who has often taken me to the lab on weekends and showed great patience and support for my work. I would also like to thank my mother and mother-in law for taking care my little baby Rui Gong in the last two years, so that I had more time to spend on research. In addition, I would like to thank my son who has given me unbelievable spiritual support. Without the support above, I could not obtain this degree.

Abstract

Utp14 recruits and activates the RNA helicase Dhr1 to undock U3 snoRNA from the pre-ribosome

Jieyi Zhu, M.A.

The University of Texas at Austin, 2016

Supervisor: Arlen Johnson

In eukaryotic ribosome biogenesis, U3 snoRNA base-pairs with the pre-rRNA to promote its processing. However, U3 must be removed to allow folding of the central pseudoknot, a key feature of the small subunit. Previously, my work contributed to showing that the DEAH/RHA RNA helicase Dhr1 dislodges U3 from the pre-rRNA. *DHR1* can be linked to *UTP14*, encoding an essential protein of the pre-ribosome, through genetic interactions with the rRNA methyltransferase Bud23. Here, I report that Utp14 regulates Dhr1. Mutations within a discrete region of Utp14 reduced its interaction with Dhr1 that correlated with reduced function of Utp14. These mutants accumulated Dhr1 and U3 in a pre-40S particle, mimicking a helicase inactive Dhr1 mutant. This similarity in the phenotypes led us to propose that Utp14 activates Dhr1. Indeed, Utp14 formed a complex with Dhr1 and stimulated its unwinding activity *in vitro*. Moreover, the *utp14* mutants that mimicked a catalytically inactive *dhr1* mutant *in vivo* showed reduced stimulation of unwinding activity *in vitro*. Dhr1 binding to the pre-ribosome was substantially reduced

only when both Utp14 and Bud23 are depleted. Thus, Utp14 is bifunctional; together with Bud23 it is needed for stable interaction of Dhr1 with the pre-ribosome and Utp14 activates Dhr1 to dislodge U3.

Table of Contents

List of Tables

List of Figures

List of Illustrations

Chapter 1 Introduction[1]

1.1 Overview

Ribosomes are fundamentally important and conserved molecular machines that translate genetic information into protein for the cells. A ribosome is a ribonucleoprotein complex that is composed of RNAs and proteins. It consists of two subunits: a small subunit (SSU) and a large subunit (LSU). In eukaryotes, the SSU sediments at 40S and contains 18S rRNA and 33 ribosomal proteins and the LSU sediments at 60S and has 5S rRNA, 5.8S rRNA, 25S rRNA and 46 ribosomal proteins (1). Each subunit has its specific function. The SSU contains the decoding center which is important for monitoring the complementarity of tRNA and mRNA, whereas the LSU has the peptidyl-transferase center which is responsible for peptide-bond formation during translation (2). The ribosomal subunits are pre-assembled in the nucleus, and undergo final maturation in the cytoplasm. These processes are very complicated and require all three RNA polymerases, more than 200 *trans*-acting factors, and highly ordered rRNA processing steps (2). Although the maturation and export of the SSU have been studied for several decades, they are still not well understood. My thesis has focused on understanding an aspect of the maturation of the SSU in the budding yeast, *Saccharomyces cerevisiae.*

[1]Chapter 1 is mainly based on previously published article: Zhu J, Liu X, Anjos M, Correll CC, Johnson AW. Utp14 Recruits and Activates the RNA Helicase Dhr1 To Undock U3 snoRNA from the Preribosome. Mol Cell Biol. 2016;36(6):965-78. PMCID: 4810474. I contributed to the whole chapter 1.

1.2 Ribosome Biogenesis

Ribosome biogenesis is a complicated and tightly regulated process. The starting point of ribosome biogenesis is in the nucleolus, a specialized compartment of the nucleus. In eukaryotes, three of the rRNAs (18S, 5.8S, and 25S/28S rRNAs) are produced from a long primary rRNA (35S) precursor transcript from the tandemly repeated ribosomal rRNA genes (about 150 copies in yeast *Saccharomyces cerevisiae*). 35S rRNA is synthesized by RNA polymerase I, while the precursor of 5S rRNA is transcribed by RNA polymerase III, and the genes of ribosomal proteins are transcribed by RNA polymerase II (3).

In yeast, the primary rRNA precursor contains a 5' external transcribed spacer (ETS), following by 18S rRNA sequence, internal transcribed spacer 1 (ITS1), 5.8S rRNA sequence, ITS2, 25S rRNA sequence, and 3'ETS. During the early transcription of the rRNA precursor, a subset of biogenesis *trans*-acting factors, ribosomal proteins and small nucleolar ribonucleoproteins (snoRNPs) associate with the nascent pre-rRNAs, to form RNPs which can be visualized as "terminal knobs" in Miller spreads (3, 4). These terminal knobs are small subunit (SSU) processomes, or 90S pre-ribosome particles, which are then split into pre-40S and pre-60S pre-ribosomal particles (5, 6).

In the process of rRNA maturation, the ETS and ITS sequences of 35S pre-rRNA have to be removed. This process is accomplished by endonucleolytic and exonucleolytic cleavage steps (Illustration 1.1). The separation of pre-40S from pre-60S subunit can be done by cleaving A0, A1 and A2 sites. After A0, A1 and A2 cleavage, 20S and 27SA2 pre-rRNA are generated. The 20S pre-rRNA, a precursor of mature 18S, is exported to cytoplasm and undergoes final cleavage at the D site by Nob1 (7). The 27SA2 pre-rRNA, a precursor for 5.8S and 25S rRNA, can be processed by two alternative pathways: cleavage at A3 followed by cleavage at B1S yields 27SB pre-rRNA; or cleavage at site

B1L, yielding 27SBL precursor. Both 27SB and 27SBL precursors undergo subsequent processing to yield mature 25S and 5.8S rRNA.

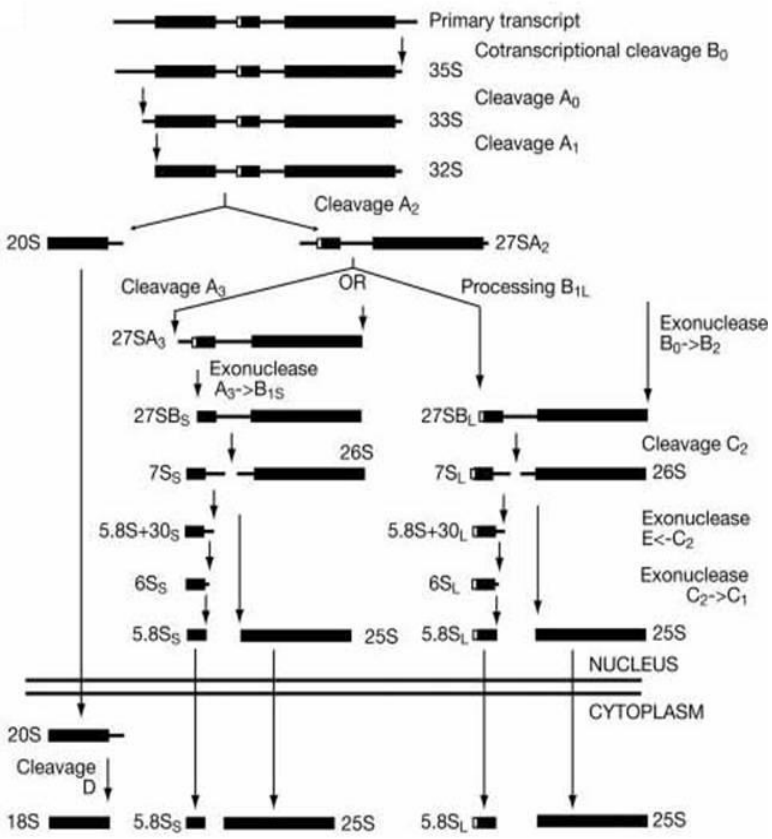

Illustration 1.1 Pre-rRNA processing scheme in *Saccharomyces cerevisiae*. **(Adapted from (8))**

1.3 The SSU processome

The SSU processome is a 2.2 MDa ribonucleoprotein complex and contains the nascent transcript of pre-rRNA, ribosome biogenesis factors, ribosomal proteins and snoRNPs (9).There are six sub-complexes that have been described: (*i*) Utp-A (U three associate protein-A) sub-complex (t-Utp4, 5, 8, 9, 10, 15, 17 and Pol5), which is required both for the transcription of the pre-rRNA and its processing, (*ii*) Utp-B subcomplex (Utp1, 6, 12, 13, 18 and 21) and (*iii*) Utp-C (Utp22, Rrp7 and the four subunits of casein kinase II: Cka1, Cka2, Ckb1 and Ckb2), which are only known to play a role in pre-rRNA processing (5, 9, 10), (*iv*) U3 snoRNP "monoparticle", (*v*) Mpp10 sub-complex and (*vi*) the Bms1/Rcl1 sub-complex. These subcomplexs join to the pre-rRNA in highly ordered fashion to ensure the accurate maturation of rRNA and ribosome assembly (11).

1.3.1 U3 snoRNA

U3 snoRNA is an evolutionarily conserved snoRNA and is instrumental in orchestrating early pre-rRNA processing (12). It belongs to the C/D box family snoRNA (Illustration 1.2) and was discovered in 1968 by James L. Hodnett and Harris Busch (13). U3 snoRNA is required for A0, A1 and A2 cleavage and can be characterized into three key domains based on its secondary structure: a 5' domain, a 'hinge' region and a 3' terminal hairpin domain (12, 14-17). The 5' domain has the conserved sequence boxes GAC, A' and A, which are involved in base-paring interactions with the pre-rRNA (14, 16, 17).

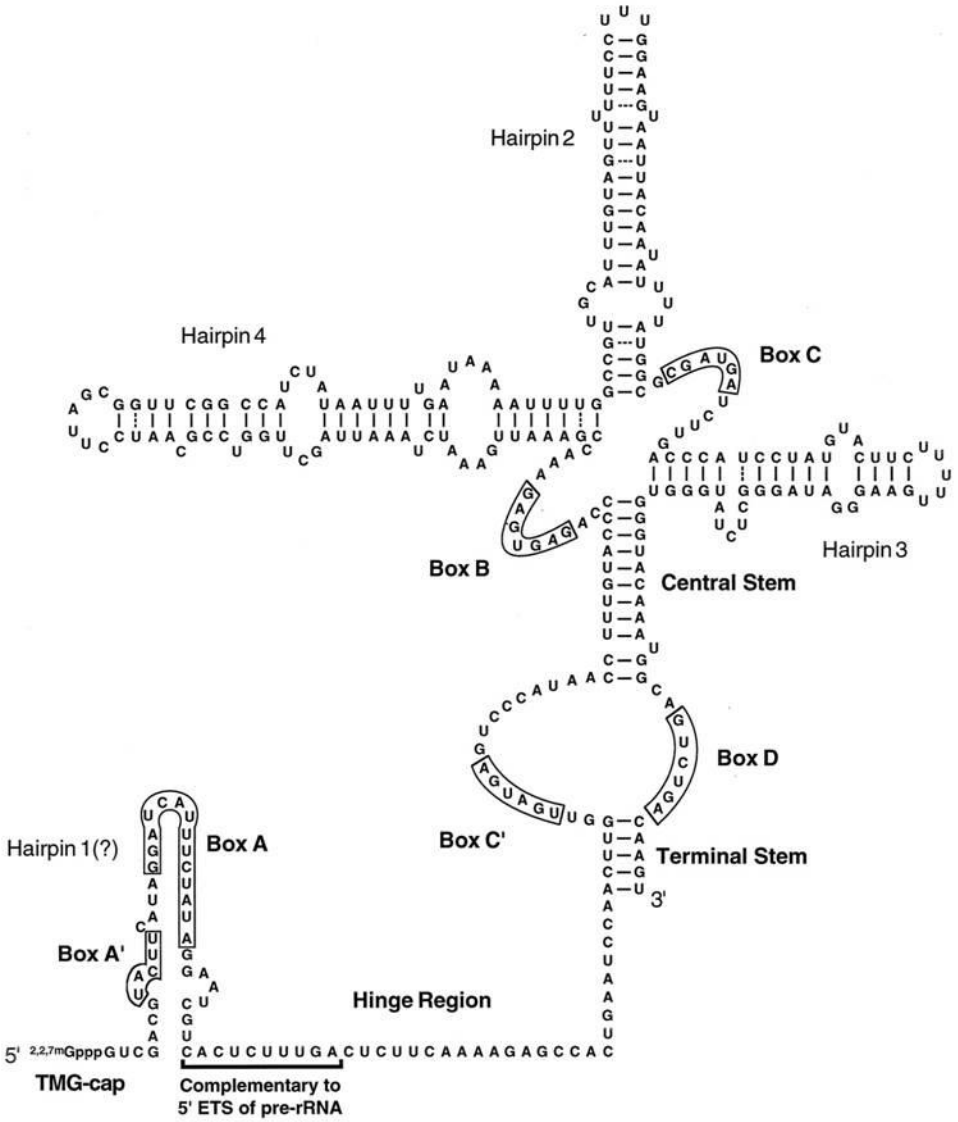

Illustration 1.2 Secondary structure of U3 snoRNA from *Saccharomyces cerevisiae.* **(Adapted from (17))**

U3 hybridizes with the pre-rRNA at multiple sites within the 35S precursor: at sites in the 5' external transcribed spacer; the 5'-end of 18S; and additional positions within 18S (12, 15, 16, 18-20). The central pseudoknot (CPK) is a key architectural feature of the small subunit (SSU) that physically coordinates the four rRNA domains and sets up the decoding

center. The CPK is formed when nucleotides (nts) in the loop of the first stem-loop structure of 18S (nts 4 to 20) base pair with nts 1137 to 1144 of 18S. In the pre-ribosome, U3 is expected to base-pair with these elements of the CPK based on genetic and phylogenetic covariation analysis (15, 16, 18, 20). However, pre-rRNA hybridization with U3 blocks the folding of the CPK. Thus, removal of U3 from the pre-ribosome is a prerequisite for, and perhaps promotes, CPK formation. We have recently shown that Dhr1, a ribosomal biogenesis factor, is responsible for removing U3 from the pre-rRNA to allow folding of the CPK (21).

1.3.2 Dhr1

There are nineteen RNA helicases that are involved in ribosome biogenesis in yeast, 17 of which are essential (21). Based on conserved sequence motifs, these helicases are characterized as either DEAD or DEAH/RHA enzymes. Dhr1 is an essential DEAH/RHA ATP-dependent RNA helicases. It is required for pre-rRNA A2 cleavage and unwinds U3 snoRNA from the pre-40S particle (21, 22). How Dhr1 activity is regulated to ensure its activity at the correct point in folding and assembly of the SSU is unknown.

Most DExD/H RNA helicases lack intrinsic regulation (23). Rather, they contain ancillary domains flanking the helicase core that provide binding sites for regulatory cofactors (23). DEAH/RHA helicases commonly use G-Patch proteins as accessory factors for activation of enzymatic activity (24). For example the yeast spliceosomal helicase Prp2 requires the G-Patch protein Spp2 and Prp43, involved in ribosome biogenesis and

spliceosome disassembly, is stimulated by at least three different G-patch proteins (Ntr1, Pfa1 and Gno1) that recruit Prp43 to its respective substrates (reviewed in 24).

To identify regulators of Dhr1 we explored candidate proteins that interact with it. The methyltransferase Bud23 modifies the guanosine base at position 1575 in 18S rRNA (25, 26). Bud23 is recruited to the pre-ribosome at a relatively late step in 40S biogenesis, before A2 cleavage, and remains associated with the pre-40S particle in the nucleus (25, 27). We took advantage of the slow growth defect of *bud23* mutants as a genetic entry point to dissect a constellation of functionally linked proteins. We found that mutations in *DHR1*, *UTP2* or *UTP14* partially suppressed the growth defect and 40S assembly defect of *bud23*Δ mutants (21, 25, 27). We also showed that Bud23 binds to the N-terminal extension of Dhr1, making Bud23 a candidate for recruiting or regulating Dhr1 (28). However, disruption of the interaction between Bud23 and Dhr1 had no observed effect on cell growth, leaving open the question of how Dhr1 is regulated.

1.3.3 Utp14

Utp14 was discovered as one of the Utp proteins of the SSU processome in yeast (9). It is required for the formation of SSU processome and maturation of the 18S rRNA (9). Although human Utp14c is reported as a retrogene, and mouse Utp14b is significant in a mouse model of male infertility, the molecular function of Utp14 has remained elusive (29). Recently, we identified a Utp14-A758G mutant that suppressed the growth defect found in *bud23*Δ yeast (27). We also found that Utp14 WT co-purified with Bud23, and the absence of *BUD23* caused mislocalization of Utp14 WT (27). Utp14 was found in 90S

particle containing the SSU processome, Mpp10, Imp4 and the U3 snoRNA, and was found in the pre-40S particle containing 20S pre-rRNA (27). In a *bud23Δ* mutant, Utp14 lost the association with the 20S pre-rRNA but not with U3, while the *utp14-A758G* mutation could partially restore the association with the 20S pre-rRNA (27). Although Utp14 has been suggested to be an ATPase, it is unlikely to be able to hydrolyze ATP because its putative Walker-A motif is not conserved when comparing the sequences of other homologs (27, 30). Therefore, the exact role of Utp14 in ribosome biogenesis remained to be identified. In this thesis, I show that Utp14 interacts directly with Dhr1 and activates its unwinding activity. My data suggest that Utp14 activates Dhr1 and together with Bud23 recruits this helicase to the assembling pre-ribosome.

Chapter 2 Materials and Methods for Chapter 3[2]

2.1 Strains, plasmids, and media.

Table 2.1 list all yeast strains used in Chapter 3. All yeast strains used in this study were grown at 30°C in YEPD (2% peptone, 1% yeast extract, 2% dextrose) or YEPgal (2% peptone, 1% yeast extract, 1% galactose) or synthetic dropout (SD) medium containing 2% glucose, unless otherwise indicated. To make AJY3243, KanMX-Gal1-3XHA was amplified from pAJ438 with AJO1948 and AJO1949. The PCR product was integrated into BY4743. After sporulation and dissection, the desired integrant was selected. AJY3245 was made by integrating *bud23Δ*:: Nat^r PCR product into AJY3243. Tables2.2 and 2.3 list all plasmids and oligonucleotides used in chapter 3, respectively.

Strain	Genotype	Source
BY4741	MATa *his3Δ1 leu2Δ0 met15Δ0 ura3Δ0*	Open Biosystems
PJ69-4α	MATα *trp1-901 leu2-3,112 ura3-52 his3Δ200 gal4Δ gal80ΔLYS2*::*GAL1-HIS3 GAL2-ADE met2*::*GAL7-LACZ*	(31)
AJY2161	MATa *bud23Δ*::*KanMX6 his3Δ1 leu2Δ0 ura3Δ0 met15Δ0*	(26)
AJY3711	MATa *KanMX6-*P_{GAL1}-3xHA-*Dhr1 his3Δ1 leu2Δ0 met15Δ0 ura3Δ0*	(21)
AJY3243	MATa*KanMX6-*P_{GAL1}-3xHA-*UTP14 his3Δ1 leu2Δ0 ura3Δ0*	This study
AJY3245	MATa*KanMX6-*P_{GAL1}-3xHA-*UTP14 bud23Δ::Natr his3Δ1 leu2Δ0 ura3Δ0*	This study
AJY3243	MATa*KanMX6-*P_{GAL1}-3xHA-*UTP14 his3Δ1 leu2Δ0 ura3Δ0*	This study
L40	MATa*his3Δ200 trp1-901, 112 ade2 LYS2::(LexAop)4-His3 URA3 (lexAop)8- LacZ Gal4*	(32)

Table 2.1 Yeast strains used in Chapter 3

[2] Chapter 2 is mainly based on previously published article: Zhu J, Liu X, Anjos M, Correll CC, Johnson AW. Utp14 Recruits and Activates the RNA Helicase Dhr1 To Undock U3 snoRNA from the Preribosome. Mol Cell Biol. 2016;36(6):965-78. PMCID: 4810474. I contributed to 2.1, 2.2, 2.4, 2.5, 2.6, 2.7.

Plasmid	Description	Source or reference
pACT2	*Gal4AD-HA LEU2 2μ*	Clontech
pAJ438	pFA6a-kanMX6-PGAL1-3HA	(33)
pAJ1918	*utp14-A758G URA3 CEN ARS*	(27)
pAJ1919	*UTP14 URA3 CEN ARS*	(27)
pAJ2311	*DHR1*-13myc *LEU2 CEN ARS*	(34)
pAJ2312	pET21a-*DHR1*-6xHis	(21)
pAJ2321	Gal4AD-HA-*UTP14LEU2 2μ*	This study
pAJ2330	Gal4BD-c-myc-*dhr1 aa1-838 TRP1 2μ*	This study
pAJ2331	Gal4BD-c-myc-*dhr1 aa319-838 TRP1 2μ*	This study
pAJ2332	Gal4BD-c-myc-*dhr1 aa319-1267 TRP1 2μ*	This study
pAJ2334	Gal4AD-HA-*utp14 aa1-706 LEU2 2μ*	This study
pAJ2335	Gal4AD-HA-*utp14 aa707-899LEU2 2μ*	This study
pAJ2341	Gal4AD-HA-*utp14 aa1-813LEU2 2μ*	This study
pAJ2342	Gal4AD-HA-*utp14 aa1-654LEU2 2μ*	This study
pAJ2343	Gal4AD-HA-*utp14 aa1-564LEU2 2μ*	This study
pAJ2344	Gal4AD-HA-*utp14 aa1-265LEU2 2μ*	This study
pAJ2345	Gal4AD-HA-*utp14 aa266-899 LEU2 2μ*	This study
pAJ2346	Gal4AD-HA-*utp14 aa565-899LEU2 2μ*	This study
pAJ2347	Gal4AD-HA-*utp14 aa655-899 LEU2 2μ*	This study
pAJ2394	LexABD-c-myc-*DHR1 TRP1 2μ*	This study
pAJ2593	*DHR1URA3 CEN ARS*	(34)
pAJ2795	Gal4AD-HA-dhr1 aa467-1267 *LEU2* 2μ	(34)
pAJ2796	Gal4AD-HA-*dhr1aa1-142 LEU2 2μ*	(34)

Table 2.2 continued next page

Plasmid	Description	Source or reference
pAJ2797	Gal4AD-HA-*dhr1aa1-467 LEU2 2μ*	(34)
pAJ2922	Gal4BD-c-myc-*DHR1*	(34)
pAJ3081	*dhr1-K420A-13myc LEU2 CEN ARS*	(21)
pAJ3132	*utp14-I755T URA3 CEN ARS*	This study
pAJ3136	*utp14-E757G URA3 CEN ARS*	This study
pAJ3145	*utp14-V754G URA3 CEN ARS*	This study
pAJ3145	*utp14-A760P URA3 CEN ARS*	This study
pAJ3263	Gal4AD-HA-*utp14 D753A V754A I755A E757A F759A LEU2 2μ*	This study
pAJ3264	*utp14-V754G I755T E757G A758G A760P URA3 CEN ARS*	This study
pAJ3265	Gal4AD-HA-*utp14 Δaa719-780 LEU2 2μ*	This study
pAJ3266	Gal4AD-HA-*utp14 V754G I755T E757G A758G A760P LEU2 2μ*	This study
pAJ3267	*utp14-Δaa719-780 URA3 CEN ARS*	This study
pAJ3276	*utp14-D753A V754A I755A E757A F759A URA3 CEN ARS*	This study
pAJ3307	pET16a-6xHis-*UTP14*	This study
pAJ3308	*UTP14*-GFP *URA3 CEN ARS*	This study
pAJ3309	*utp14 V754G I755T E757G A758G A760P -GFP URA3 CEN ARS*	This study
pAJ3310	*utp14 D753A V754A I755A E757A F759A -GFP URA3 CEN ARS*	This study
pAJ3313	*utp14 Δaa719-780 -GFP URA3 CEN ARS*	This study
pAJ3314	pET16a-6xHis-*utp14 Δaa719-780*	This study
pAJ3315	pET16a-6xHis-*utp14 D753A V754A I755A E757A F759A*	This study
pAJ3331	6xHis-*UTP14 URA3 CEN ARS*	This study
pAJ3421	*utp14 aa1-813 URA3 CEN ARS*	This study

Table 2.2 continued next page

Plasmid	Description	Source or reference
pAJ3422	*utp14 aa1-706 URA3 CEN ARS*	This study
pAJ3423	*utp14 aa1-654 URA3 CEN ARS*	This study
pAJ3424	*utp14 aa1-564 URA3 CEN ARS*	This study
pAJ3425	*utp14 aa1-265 URA3 CEN ARS*	This study
pAJ3426	*utp14 aa266-899 URA3 CEN ARS*	This study
pAJ3427	*utp14 aa565-899 URA3 CEN ARS*	This study
pAJ3428	*utp14 aa655-899 URA3 CEN ARS*	This study
pAJ3429	*utp14 aa707-899 URA3 CEN ARS*	This study
pAJ3455	*dhr1 aa319-1267 URA3 CEN ARS*	This study
pAJ3456	*dhr1 aa467-1267 URA3 CEN ARS*	This study
pAJ3457	*dhr1 aa1-838 URA3 CEN ARS*	This study
pAJ3458	*dhr1 aa1-142 URA3 CEN ARS*	This study
pAJ3459	*dhr1 aa1-467 URA3 CEN ARS*	This study
pAJ3460	*Gal4BD-c-myc-dhr1 aa584-1267 TRP1 2μ*	This study
pAJ3461	Gal4BD-c-myc-dhr1 aa839-1267 *TRP1* 2μ	This study
pAJ3470	*dhr1 aa319-838 URA3 CEN ARS*	This study
pGBKT7	*Gal4BD-c-myc TRP1 2μ*	Clontech

Table 2.2 Plasmids used in Chapter 3

Oligonucleotide	Target(s)	Sequence
AJO603	35S, 27SA2, 23S, 21S	TGTTACCTCTGGGCCCCGATTG
AJO130	20S	TCTTGCCCAGTAAAAGCTCTCATGC
AJO962	U2	GCGACCAAAGTAAAAGTCAAGAACGACTCCACAAG TGCGAGGGTCGCGAC
AJO2194	U3	CTCATCAACCAAGTTGGATTCAGTGGCTC
AJO944	Utp14	CATAAACTGGACAGTGTTTTCTTCAGACTTTTTATG
AJO1399	Utp14	ATCACCCATCTCACTCAACTTATCC
AJO1948	Utp14	TCATTAAGTGTGCATTCAATAACATCTTGTTATATA CTAATAAAAGAGGCGAATTCGAGCTCGTTTAAA
AJO1949	Utp14	TCCAAAACTCTTCTAGAACTCTTGGATCTGCTCTTA GATTTCTTTTTTGCGCACTGAGCAGCGTAATCTG

Table 2.3 Oligonucleotides used in Chapter 3

2.2 Yeast two-hybrid assays

To test the interaction of Dhr1 and Utp14 by yeast two-hybrid assay, WT and mutant *DHR1* and *UTP14* genes were amplified by PCR using specific pairs of oligonucleotides that are listed in Table 3. The PCR products were cut with restriction enzymes and were ligated to either pACT2, pGBKT7 orpAJ2394 two-hybrid vectors which were also cut with corresponding restriction enzymes. Plasmids were confirmed by sequencing. WT or mutant Utp14 was cotransformed with WT Dhr1 into PJ69-4α (31) or L40 (32). WT or mutant Dhr1 was cotransformed with WT Utp14 into PJ69-4α (31) or L40 (32). Transformants were selected on SD Leu− Trp− medium and then patched on SD Leu− Trp− His− with or without 3-Amino-1,2,4-triazole (3-AT) to test for activation of UAS_{GAL}-HIS3 or $(LexAop)_4$-HIS3 reporter genes. These plates were incubated at 30°C for 48-72 h.

2.3 Screen to identify additional mutants of *UTP14* as suppressors of the*bud23Δ*mutant.

To indentify additional mutants of *UTP14* that suppressed a *bud23Δ*mutant, *UTP14* was amplified by PCR using oligonucleotides AJO944 and AJO1399 with *Taq* DNA polymerase. The PCR product was cotransformed with *Hpa*I and *Aat*II-digested pAJ1919 into the *bud23Δ* mutant strain (AJY2161). The transformants were selected on SD Ura− medium at 30°C for 48-72 h. Plasmids were isolated from fast-growing clones and sequenced (28).

2.4 Northern blot analysis

2.4.1 RNA preparation

To prepare total RNA, all yeast cultures were grown at 30°C to a density of ~$1x10^7$ cells/ml and RNA was prepared using the hot acidic phenol method (35). For RNA isolation from sucrose gradient fractions, 1/10 volume of 20% SDS, 1/10 volume of 3M Na Acetate (pH5.5) and 2.375 volumes 100% ethanol were added to each fraction and stored at -20°C for 24h. The RNA was collected by centrifugation at 14,000 rpm at 4°C for 30 min. The RNA pellet was washed once with 70% ethanol, and resuspended in DEPC-treated ddH_2O.

2.4.2 Gel and blotting

For gel analysis of RNAs, a defined quantity of RNA samples were dried by vacuum for 20 min in a SpeedVac. The RNA pellet was resuspended by RNA sample buffer (50% deionized formamide, 16% 37% formaldehyde, 1X MOPS) and heated at 68°C for 15 min. RNA dye was added to the samples on ice. Samples were separated on a 1.2% agarose formaldehyde gel at 50V for 3 h at room temperature. The gel was rinsed with DEPC ddH_2O 3 times, shaking for 10 min each, incubated in 1X SSC for 20 min and transferred to Zeta probe nitrocellulose membrane by downward capillary transfer using the Schleicher & Schuell Truboblotter transfer system. After overnight transfer, the membrane was soaked in 20X SSC for 5 min, and crosslinked twice using a Stratagene UV Stratalinker 1800 at auto-crosslink setting.

2.4.3 Hybridization

Membranes with RNA were pre-incubated with hybridization solution (5X SSC, 20mM Na_2HPO_4 pH7.2, 7% SDS, 1X Denhardt's, 100μg/ml Denatured herring sperm DNA) for 30min at 50°C in the hybridization oven with rotation. The hybridization solution was removed and replaced with the same buffer. Radiolabled probes that listed in Table 3 were added and hybridization was carried out at 50°C for 24 h. The membrane was washed twice with wash solution 1 (3X SSC, 10X Denhardt's, 5% SDS, 25mM NaH_2PO_4 pH 7.5) and washed once with wash solution 2 (1X SSC, 1% SDS). The blotted membrane was then exposed to a phosphor screen for 2 h, the screen was scanned with a Typhoon FLA9500 and the image was analyzed by Image J.

2.5 Sucrose density gradient sedimentation.

Fresh overnight cultures were innoculated into 250ml SD or YPD media to give 0.1 OD600 and were grown at 30°C to a density at of ~$1x10^7$ cells/ml. Cycloheximide was added to a final concentration of 100 µg/ml and the cultures were incubated at 30°C shaker for 10 min. The cells were then immediately poured onto centrifuge bottles over ice and collected by centrifugation at 5,000 rpm for 5 min in a Beckman JLA-10.5 rotor. Cells were then stored at -80°C. To make the cell lysate, cells were thawed on ice and washed with lysis buffer (50 mM Tris-HCl pH 7.5, 100 mM KCl, 5 mM $MgCl_2$, 7 mM β-mercaptoethanol, 100 µg/ml cyclohexamide, 1X pepstatin-A, 1X leupeptin, and 1 mM PMSF). Cells were resuspended in an equal volume of lysis buffer, glass beads were added to 2/3 volume of the cell suspension and cell membranes were lysed by vortexing 30 sec for seven times using VWR vortex-genie 2 set to maximum speed with 1min 30sec interval on ice. Extracts were then clarified by centrifugation at 14,000 rpm for ten minutes at 4°C. The supernatant was collected and transferred to a pre-chilled new tube. The OD_{260} of the cell extract was measured and 9 A_{260} units was loaded onto a sucrose gradient (7%-47%) and centrifuged at 40,000 rpm for 2.5 h using Beckman SW40 rotor. The gradients were fractionated using an ISCO model 640 density gradient fractionator while monitoring absorbance at 254 nm. To precipitate proteins from fractions, trichloroacetic acid (TCA) was added to 1/10 volume of the fraction. These samples were stored at −20°C for 24 h. Precipitated proteins were collected by centrifugation at 4°C and 14,000 rpm for 20min. The pellets were resuspended in 1X Laemmli buffer with Tris and heated at 99°C for 3

min, and then were store at -80°C or separated on 8% SDS-PAGE gels. Proteins were transferred to a nitrocellulose membrane with Towbin buffer (25 mM Tris, 192 mM glycine, 20% methanol, 0.1% SDS, pH 8.3) or CAPS buffer (10 mM N-cyclohexyl-3-aminopropanesulfonic acid, 10% methanol, pH 11) and subjected to Western blot analysis.

2.6 Immunoprecipitation

Fresh overnight cell cultures were diluted into 300 ml of ura- leu- galactose media to OD_{600} at 0.1. Glucose was added to the culture to final concentration at 2%, and continued growth for 6 h at 30°C. Cells were harvested and stored at -80°C. Cells were thawed on ice and whole cell extracts were prepared in IP buffer (50 mM Tris-HCl pH 7.5, 100 mM NaCl, 1.5 mM $MgCl_2$, 0.15% NP40, 1 mM PMSF, 1 μg/ml leupeptin, 1 μg/ml pepstatin A) by vortexing with glass beads, and clarifying by centrifugation at 14,000*g* at 4°C.Extracts were normalized by OD_{280}, Placental RNase inhibitor (New England Biolabs) was added to the samples and sample were incubated with Protein-G magnetic beads (New England Biolabs) pre-bound with anti-GFP antibody for 2 h at 4°C. The beads were washed with IP buffer three times for 5 min each at 4°C. Proteins and RNA were extracted from the beads with equal volume of LETS (10 mM Tris-HCl, pH7.4, 100 mM LiCl, 10 mM EDTA and 0.2% SDS) and acid-phenol: chloroform. The aqueous phase was re-extracted with acid-phenol: chloroform. The final aqueous phase was precipitated with 2.5 volumes 100% ethanol and 1μl of 5 mg/ml glycogen (Ambion) overnight at -20°C. RNA was recovered by centrifugation, pellets washed with cold 70% ethanol, and northern blot analysis was performed. Proteins were recovered from the organic phase from the first

extraction by precipitation with acetone. Proteins were eluted in 1X Laemmli buffer and separated on 8% SDS-PAGE gels. Proteins were transferred to a nitrocellulose membrane with CAPS buffer and subjected to Western blot analysis.

2.7 Western blot analysis

Membranes were blocked with 5% milk in 1X TBS for 30 min at room temperature, and washed with 1X TBS 3 times for 5 min each. Membranes were then incubated with primary antibody diluted in 1X TBST with 1% milk for 2 h at room temperature. Primary antibodies used here were polyclonal rabbit anti-GFP antibody (1:5000, M. Rout), monoclonal mouse anti-c-myc antibody (9e10, 1:10,000, Biolegend), polyclonal rabbit anti-Mpp10 antibody (1:10,000, S. Baserga), polyclonal guinea pig anti-Imp4 antibody (1:3000, S. Baserga) and monoclonal mouse anti-HA antibody (1:5000). Membranes were washed with 1X TBST 3 times for 5 min each, and then were incubated with secondary antibodies in 1X TBST with 1% milk for 30 min at room temperature. Secondary antibodies used here were polyclonal goat anti-mouse, goat anti-rabbit and goat anti-guinea pig HRP-coupled antibodies (1:30,000), anti-mouse and anti-rabbit fluorescent-coupled antibodies. Membranes were washed with 1X TBST 3 times for 5 min each. Finally, ECL solution (Thermo Scientific) was added on the surface of membranes which were then exposed to X-ray film. Membranes which contained the fluorescent signal were detected by Li-Cor Odessy. The images were analyzed with Li-Cor Image studio software.

2.8 Protein expression and purification

Dhr1 and Dhr1$_{D516A/E517A}$ were expressed and purified as described before (21). His6-Utp14, His6-Utp14$_{multi-Ala}$ and His6-Utp14$_{\Delta 719-850}$were expressed from pAJ3307, pAJ3315 and pAJ3314, respectively, overnight at 15°C in BL21 Star (DE3) (Life Technologies) cells supplemented with a vector expressing the tRNA genes *argU*, *ileY* and *leuW*. Cells were washed once and resuspended with extraction buffer (50 mM Tris-HCl pH 8.0, 500 mM NaCl, 10% [v/v] glycerol, 5 mM BME, 7 units/ml RNase A and 10 units/ml RNase I). The extensive RNase treatment ensured the removal of tightly bound RNA. A French Press was used to lyse cells and cell extracts were clarified for 10 min at 10,000*g* followed by 30 min at 50,000*g*. Supernatant was loaded on Ni-NTA resin (Invitrogen) and washed once with extraction buffer without RNase. The resin was then resuspended with 3 column volumes (CV) of extraction buffer and incubated 15 min. The resin was washed extensively with extraction buffer without RNase and protein was eluted with extraction buffer in which NaCl was replaced with 250 mM imidazole. Fractions containing Utp14 were pooled, supplemented with 1 mM DTT, and applied to CM Hitrap column (GE Healthcare Life Sciences). The column was washed with Buffer A (30 mM Tris pH 8.0, 5% [v/v] glycerol, 5 mM sodium acetate, and 1 mM DTT). Protein was eluted with a 21 CV gradient from 0% to 60% buffer B (buffer A plus 1 M NaCl). Utp14 containing fractions were pooled, dialyzed (30 mM Tris pH 8.0, 10% [v/v] glycerol, 5 mM sodium acetate, 150 mM NaCl, and 1 mM DTT), and concentrated to ~5 μM. Aliquots

were flash frozen and stored at −80°C. Yield for WT and mutant Utp14 was approximately 1 mg/liter.

2.9 Preparation of Dhr1: Utp14 complex

All reactions were performed at RT. To test the binding of Utp14 and Dhr1, 2 μM of Dhr1 with or without 2 μM Utp14 WT and mutants was first pre-incubated for 5 min, then bis[sulfosuccinimidyl] substrate (BS^3) was added to a concentration of 2 mM. The reactions were incubated for 30 min then stopped by addition of 200 mM Tris [pH 8.0]. The reaction mix was analyzed by SDS-PAGE or mass-spec.

2.10 Mass-Spectrometric Analysis

Protein samples were subjected to analysis by surface enhanced laser desorption and ionization-time-of-flight (SELDI-TOF) mass spectrometry to examine the distribution of masses of protein components. Samples were spotted in three successive 2 μl aliquots onto individual spots of a ProteinChip H50 Array (BioRad) and allowed to partially air dry for one hour or overnight between applications. The chip was then washed three times with 5 μl distilled water and with 5% MeOH respectively and air-dried prior to the addition of 3 μl of 10 mg/ml sinapinic acid (BioRad) in 60% acetonitrile/0.1% formic acid. Controls omitting the air drying for multiple applications of the sample as well as omitting the formic acid with matrix crystallization indicated no difference in the distribution of multimers (data not shown). Samples were analyzed using a BioRadProteinChip System 4000 Enterprise mass spectrometer calibrated against BioRad's Protein Standards. The

acquisition mode was positive with source at 25 kV. The matrix attenuation was set up as 500 Da. The sampling rate was 800 MHz. Each spot was divided into 10 partitions with 210 shots/partition and the data were collected at a laser energy of 3300 nJ with a mass range between 10-200 kDa.

2.11 RNA substrates

U3 snoRNA was transcribed as previously described (36, 37) and purified by gel electrophoresis and refolded. ETS2 (5'-GGA UUU GGU GG-3') was purchased from IDT. The 5'-end of ETS2 was phosphorylated with γ-[32P]-ATP (PerkinElmer, 150 μCi/μL) by T4 Polynucleotide Kinase (New England Biolabs). Radiolabeled ETS2 was purified by gel electrophoresis, precipitated by ethanol, resuspended in water, and stored at −20°C. Poly(A) was purchased from SIGMA.

2.12 ATPase assay

ATPase assays were performed as described before (21), except some reactions included 0.5 μM Utp14 and final reaction conditions were 1 mM ATP, 1 mM $MgCl_2$, 32 mM Tris (pH 8), 60 mMNaCl, 4% glycerol, 2 mM sodium acetate and 2.4 mM DTT.

2.13 Unwinding reactions

All unwinding reactions were performed at room temperature. Pre-steady state reactions: to form the U3-ETS2 duplex, bottom strand U3 snoRNA was incubated for 20 min at 45°C, then refolded on ice for 10 min, and subsequently annealed with ^{32}P-ETS2 at

room temperature for 10min. The reaction was further incubated 10 min with buffer supplemented with $MgCl_2$ at room temperature. The pre-formed U3-ETS2 duplex was incubated with Dhr1 (WT or mutant) in the presence or absence of Utp14 (WT or mutant) for 5 min and reactions were initiated by rapid addition of 1 mM mixture of ATP and $MgCl_2$. The final concentrations were 1 mM ATP, 1.5 mM $MgCl_2$, 1.5 nM bottom strand RNA, ≤0.3 nM ^{32}P ETS2, 50 nM Dhr1, in the presence or absence of 200 nM Utp14, 20-35 mM Tris (pH 8.0), 50 mM NaCl, 7% (v/v) glycerol, 2.7 mM DTT, 0.8 units/µl RNasin, and 0.2 mg/ml BSA. Reactions were sampled and quenched by addition of one-half volume of stop buffer (150 mM Tris [pH 8.0], 0.3% [w/v] SDS, and 150 mM EDTA). The amount of duplex and single stranded RNA for both of the above helicase reactions were resolved by electrophoretic mobility shift assays (EMSAs).

Charter 3 Results[3]

3.1 Utp14 and Dhr1 Interact by yeast 2-hybrid analysis

In our previous work, we identified multiple Dhr1 mutants and a single Utp14 mutant that suppressed the growth defect of *bud23*Δmutant yeast. Based on the functional interactions of these proteins, I wanted to examine the potential physical interaction between Dhr1 and Utp14. I performed yeast two-hybrid studies and detected a robust interaction between these proteins (Figure 3.1). Next, I wanted to find out which region of Dhr1 is needed for this interaction. I first made a series of truncations. Dhr1can be divided into functional domains based on sequence homology and by extension of structural homology to Prp43 (38, 39) (Figure 3.1), which we used to construct a model (Figure.3.2). In our previous study, we found that the N-terminal domain (amino acids [aa] 1 to 356) contains a binding site for Bud23 (28). This domain is followed by the helicase core (aa 375 to 839) composed of tandem RecA-like domains, designated RecA1 and RecA2. The core is followed by a winged helix domain (aa 840 to 905), a ratchet domain (aa 906 to 1056), an OB fold (aa 1057 to 1192) and a small C-terminal extension (aa 1193 to 1267). Deletion of the N-terminal domain of Dhr1 had no effect on its interaction with Utp14 (Figure 3.1). However, deletion of an additional 148 aas, extending into the RecA1 domain, or larger deletions, completely eliminated the two-hybrid interaction (Figure3.1).

[3]Chapter 3 is mainly based on previously published article: Zhu J, Liu X, Anjos M, Correll CC, Johnson AW. Utp14 Recruits and Activates the RNA Helicase Dhr1 To Undock U3 snoRNA from the Preribosome. Mol Cell Biol. 2016;36(6):965-78. PMCID: 4810474. I contributed to 3.1, 3.3,, 3.5, 3.6, 3.9.

Likewise, deletion of the winged helix domain through the C-terminus completely eliminated two-hybrid interaction. I also checked the protein expression level by Western blotting and confirmed that all truncations were expressed as well as the wild-type protein (Figure 3.3).

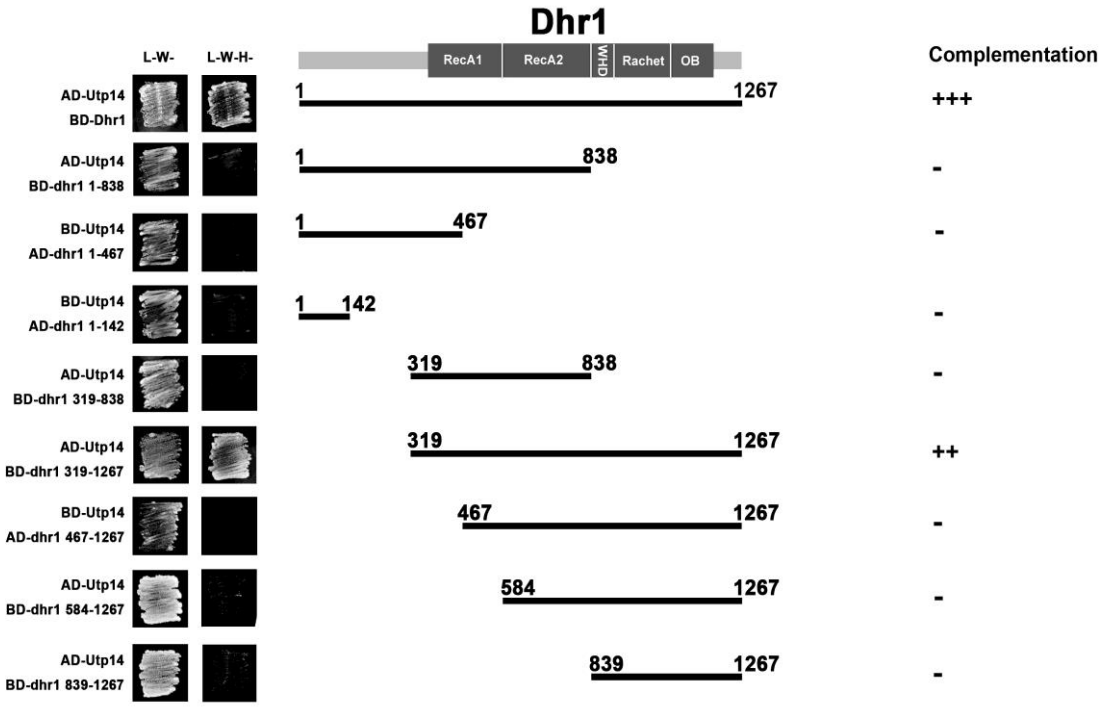

Figure 3.1 Mapping the Dhr1-Utp14 interaction and mapping the Dhr1 binding site on Utp14 by yeast two-hybrid.

Cartoon of domain organization of Dhr1. Strain PJ69-4α was transformed with Gal4AD-Utp14 and a second plasmid encoding Gal4BD fusions of either full-length Dhr1, or truncated proteins containing aa1-813, aa319-838 and aa319-1267. The truncated Dhr1 mutant proteins, aa1-467, aa1-142 and aa467-1267, were fused with Gal4AD and were co-expressed with Gal4BD-Utp14 in PJ69-4α. The transformants were patched on SD lacking either leucine and tryptophan (L-W-), or lacking leucine, tryptophan and histidine (L-W-H-) media and incubated for 3 days at 30°C.

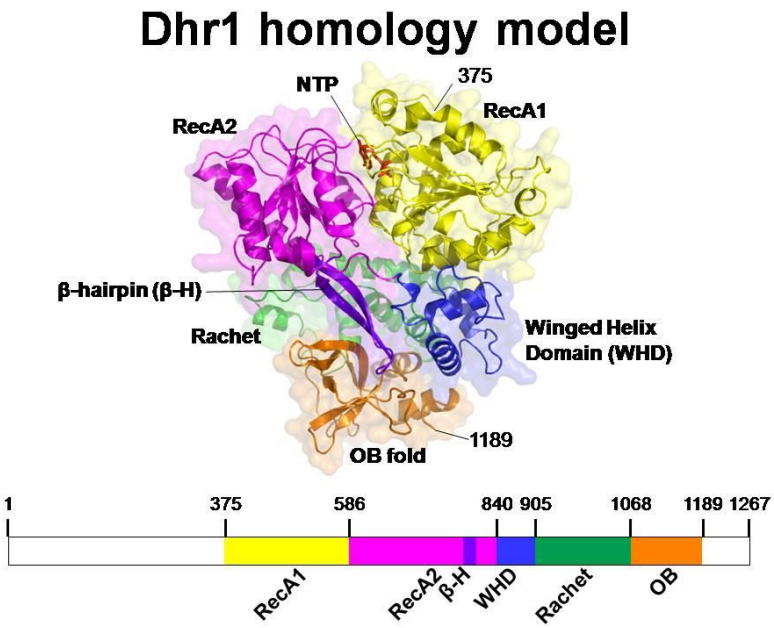

Figure 3.2 Homology model of Dhr1.

Amino acids 375 to 1189 of Dhr1 were modeled on the structure of Prp43 (pdb 3KX2) using Phyre2 (40). The structure of residues 1 to 374 and 1190 to 1267 is unknown. The model of Dhr1 contains two RecA-like domains (RecA1 and RecA2), a feature shared by DEAD-box and viral DExH helicases. The two RecA-like domains are involved in ATP binding and hydrolysis and duplex binding. RecA2 also contains a β-hairpin. Downstream of the RecA-like domains there is winged-helix domain (WHD) followed by a rachet domain, similar to the processive DNA helicase Ski2-like Hel308. The C-terminal region of Dhr1 contains an oligonucleotide/oligosaccharide-binding (OB) motif.

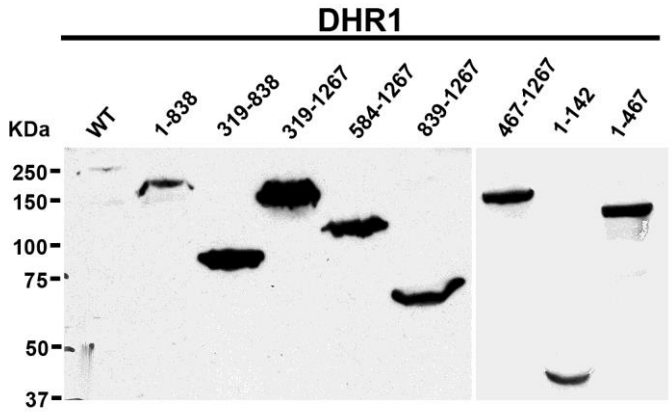

Figure 3.3. Expression level of Dhr1 two-hybrid proteins.

The protein level of Dhr1 truncated mutants. Gal4BD or Gal4AD fusions of either full-length DHR1 or truncated mutants were transformed in PJ69-4α. Cells were lysed with NaOH (41). The extract was separated with 8% SDS-PAGE, and subjected to western blotting using anti-myc or anti-HA antibodies.

This result was demonstrating that loss of two-hybrid interaction was not because of poor expression of the mutant proteins. Thus, all but the N-terminal domain of Dhr1 (aas 1 to 318) is needed for two-hybrid interaction with Utp14. The winged helix, ratchet domain and OB fold are expected to create a base to orient the tandem RecA-like domains. Therefore, a relatively compact region of Utp14 could interact with disparate domains of Dhr1. I also tested these truncations of Dhr1 for their ability to complement loss of Dhr1 (Figure 3.1 and Figure 3.4). Dhr1 lacking the N-terminus weakly complemented loss of Dhr1. Further deletions into the RecA-like domains or deletion of the remaining C-terminal region completely inactivated the protein.

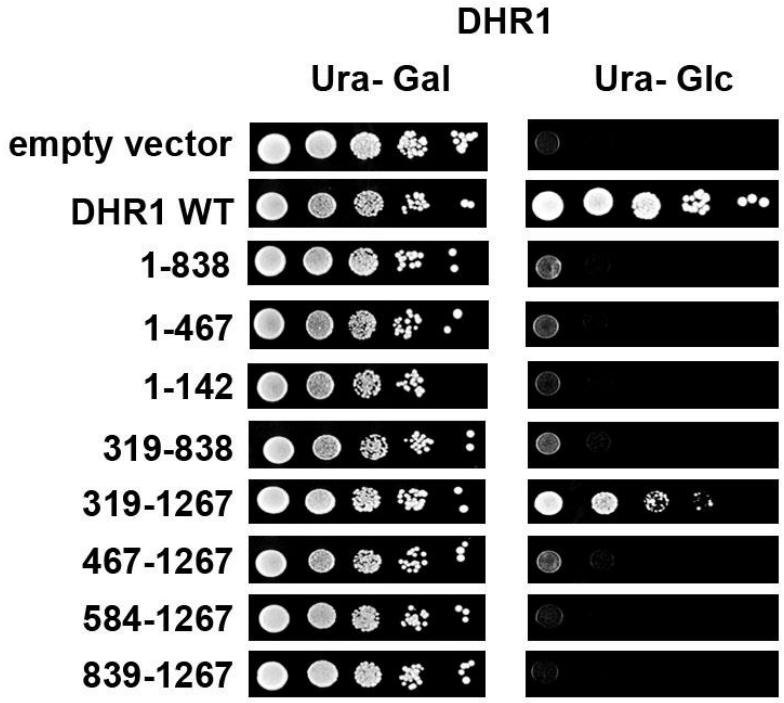

Figure 3.4 Complementation of *DHR1* truncated mutants.

Empty vector, full-length *DHR1* or truncated mutants were transformed into PGal1-DHR1 strain (AJY3711) and grown on SD Ura- glucose medium and SD Ura- galactose for 4 days at 30°C.

In contrast to Dhr1, Utp14 has no structural homologs and thus no identifiable sequence motifs suggesting functions for Utp14. However, there are regions of strong conservation in the N-terminus (~aa 180 to 520) and in the C-terminus (~aa 750 to 895) (Figure 3.5). To narrow down the region of Utp14 that interacts with Dhr1, I made serial N- and C-terminal truncations (Figure 3.5). I tested these in two-hybrid assays with full length Dhr1 and titrated with 3 amino triazole (3AT) to better differentiate relative strengths of interaction (31). $Utp14_{1\text{-}813}$ and $Utp14_{1\text{-}706}$ (deleting 86 and 193 aas, respectively, from the C-terminus) showed increasingly severe reductions in two-hybrid interaction with Dhr1 and larger deletions showed no detectable interaction (Figure 3.5). $Utp14_{266\text{-}899}$ (deletion of 265aas from the N-terminus) had no discernable effect on Dhr1 interaction whereas $Utp14_{565\text{-}899}$ and $Utp14_{655\text{-}899}$ (deletion of 564 and 654aas, respectively, from the N-terminus) gave increasingly severe loss of interaction. These results show that aas 565 to 813 of Utp14 are necessary for efficient two-hybrid interaction with Dhr1.

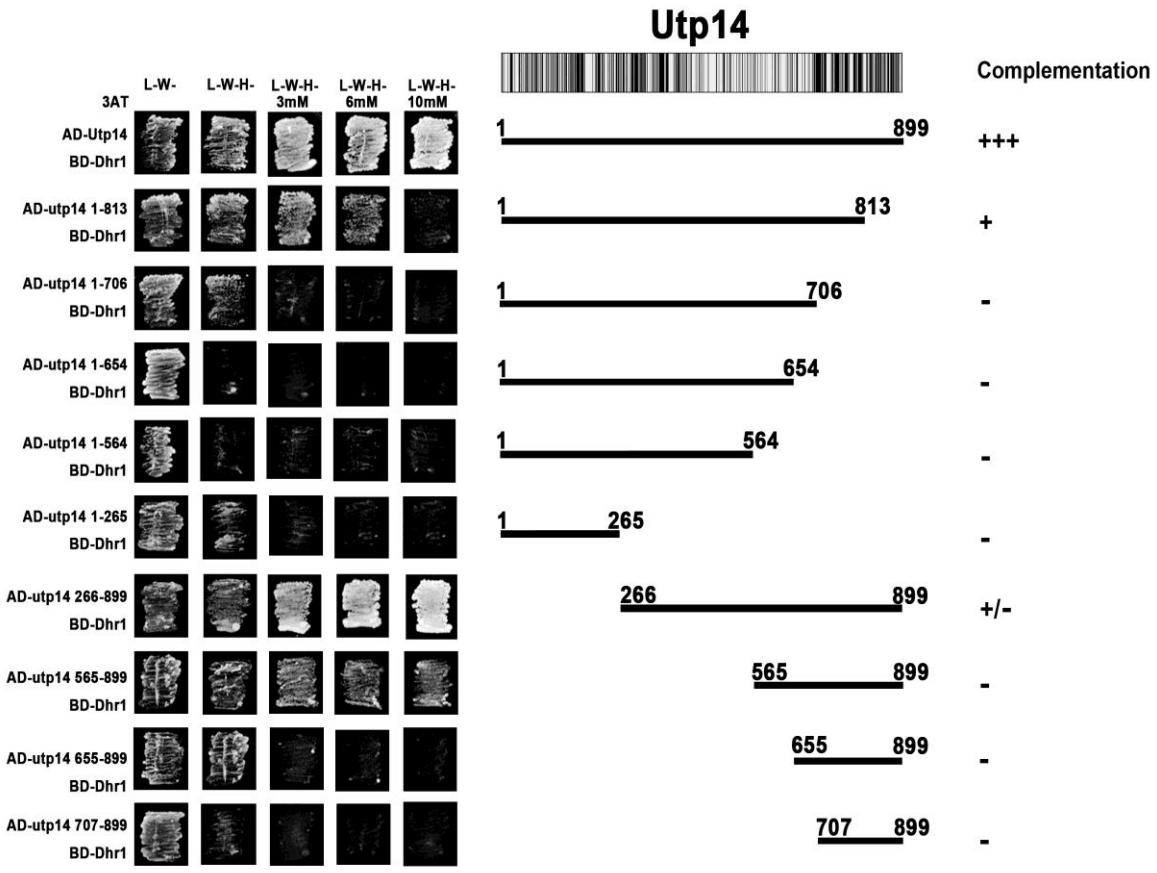

Figure 3.5Mapping the Utp14 binding site on Dhr1by yeast two-hybrid.

Cartoon of amino acid conservation of Utp14. Multiple sequence alignment was done with Geneious software. Black: 100% identity; dark gray: 80-100% similarity; light gray: 60-80% similarity; white <60% similarity. Strain PJ69-4α was transformed with Gal4BD-Dhr1 and a second plasmid encoding Gal4AD fusions of either full-length Utp14, or truncated Utp14. The transformants were patched on SD L-W-, SD L-W-H-, and SD L-W-H-media with different concentrations of 3AT and incubated for 3 days at 30°C.

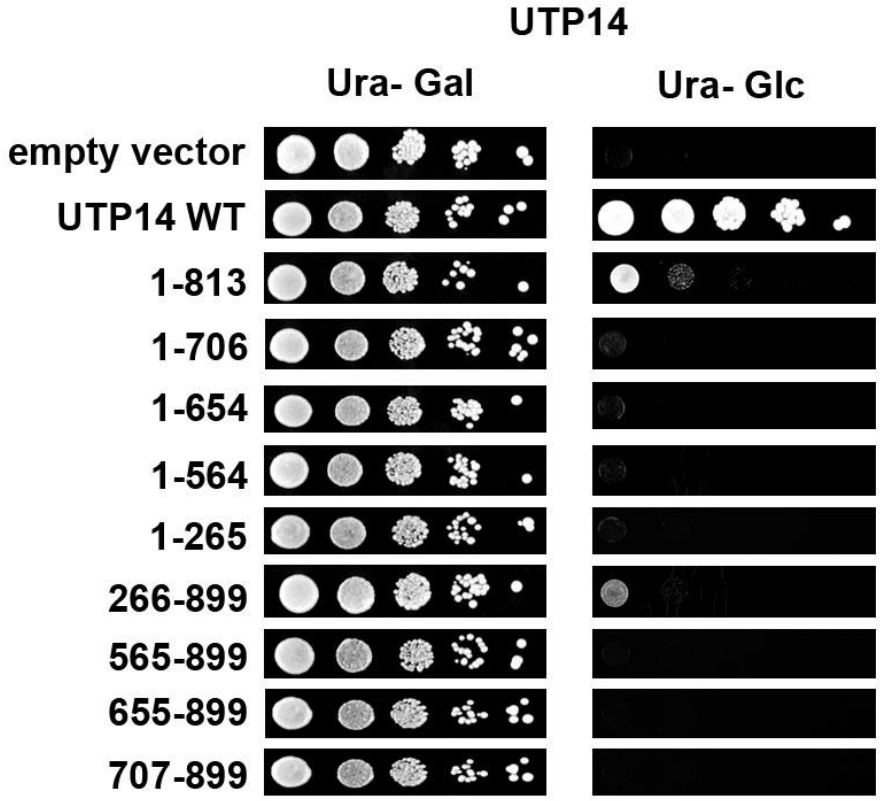

Figure 3.6. Complementation of *UTP14* truncated mutants.

Empty vector, full-length *UTP14* or truncated mutants were transformed into PGal1-UTP14 strain (AJY3243), grown on SD Ura- glucose medium and SD Ura- galactose for 4 days at 30°C.

3.2 Mutations in *UTP14* that suppress *bud23*Δ map to a highly conserved peptide in the C-terminus of Utp14

A previous lab member, Joshua P. White, found that an alanine to glycine substitution at position 758 in Utp14 suppressed the growth and rRNA processing defects of *bud23*Δ (27). To better define the functional domain of Utp14 important for *bud23*Δ suppression, Margarida Anjos screened for additional suppressing mutations. She randomly mutagenized the entire open reading frame of *UTP14* by PCR and recombined the mutant product into a *UTP14* expression vector in *bud23*Δ cells. She assumed that additional suppressing mutations in *UTP14* could be identified in the presence of genomic WT *UTP14* because $UTP14_{A758G}$ is a dominant suppressor. Therefore, fast growing colonies were isolated and *UTP14* was sequenced to identify suppressing mutations. In cases where multiple mutations were identified, she subcloned these to identify the specific mutation conferring suppression. She identified four additional unique mutations that suppressed *bud23*Δ: V754G, I755T, E757G and A760P (Figure 3.7). All single point mutations suppressed *bud23*Δ to a similar extent (Figure 3.8A) and all fully complemented loss of Utp14 (Figure 3.8B). The clustering of mutations identified a short highly conserved peptide as a functionally important element of Utp14.

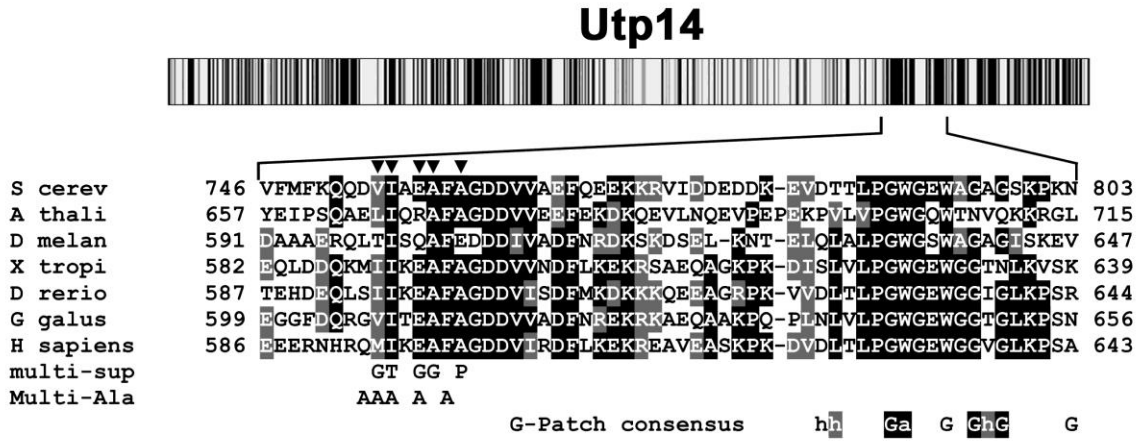

Figure 3.7 Suppressing mutations map to a highly conserved motif in Utp14.

Cartoon showing conservation of amino acid sequence across Utp14 (upper panel) as described in the legend to Figure 1. Multiple sequence alignment of the region of Utp14 containing mutations that suppress *bud23*Δ (lower panel) was performed with T-coffee. S cerev, Saccharomyces cerevisiae; A thali, Arabidopsis thaliana; D melan, Drosophila melanogaster; X tropi, Xenopus tropicalis; D rerio, Danio rerio; G galus, Galus galus; H Sapiens, Homo sapiens. Positions of single amino acid substitutions that suppress *bud23*Δ are indicated by (▼). The amino acid changes of Utp14multi-Sup and Utp14multi-Ala are indicated. The consensus sequence of G-Patch proteins is shown below the alignment. Perfect matches with invariant residues are shaded in black and similar residues shaded in gray.

3.3 Combining suppressing mutations or deletion of the region containing the mutations impairs Utp14 function

Individually, the mutations in Utp14 fully complemented loss of Utp14 and therefore are expected to only slightly perturb a protein-protein or protein-RNA interaction to suppress *bud23*Δ. To make more severely disruptive mutants I combined multiple suppressing mutations ($Utp14_{multi\text{-}sup}$), changed multiple residues within this motif to

alanine ($Utp14_{multi\text{-}Ala}$) or deleted this region entirely ($Utp14_{\Delta 719\text{-}780}$) which was done by Margarida Anjos. I tested whether these additional mutants had more severe phenotypes than the single point mutations. Indeed, these mutants displayed a gradation of function in the order: WT, $Utp14_{multi\text{-}sup}$, $Utp14_{multi\text{-}Ala}$, and $Utp14_{\Delta 719\text{-}780}$, which was lethal (Figure 3.8B). None of the three mutants suppressed *bud23*Δ (Figure 3.8A). These more disruptive *utp14* mutants allowed us to separate functions of Utp14 that could not be done with a complete loss of function mutant.

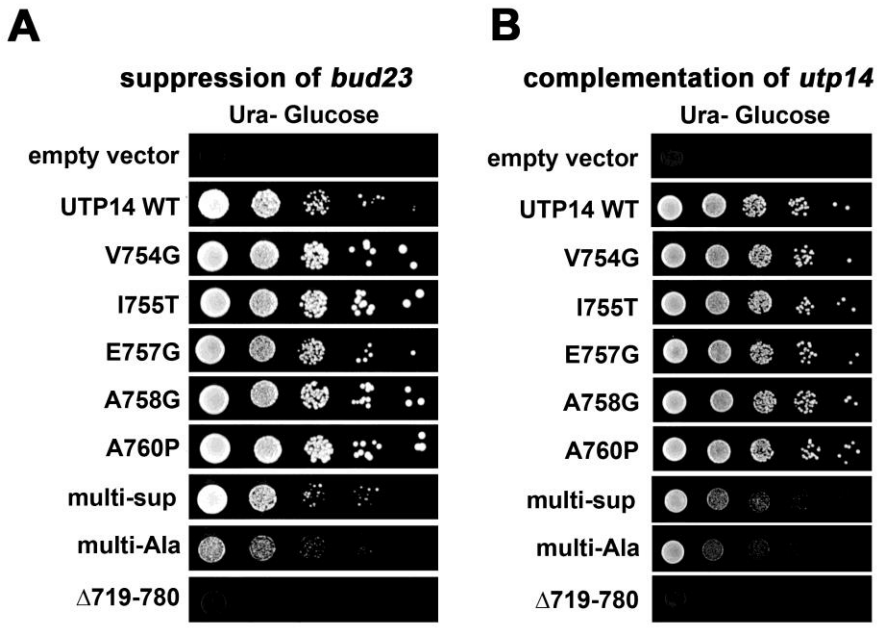

Figure 3.8 Suppression and complementation assays of Utp14 suppressing mutants.

(A) WT UTP14 or indicated mutants were expressed in a *bud23*Δ PGAL1-UTP14 strain AJY3245 and 10-fold serial dilutions of cells were spotted onto glucose-containing medium and grown for 2 days at 30°C. (B) WT UTP14 or indicated mutants were expressed in a PGAL1-UTP14 strain AJY3243 and 10-fold serial dilutions of cells were spotted onto glucose-containing medium and grown for 2 days at 30°C.

3.4 Impaired function of Utp14 correlates with loss of Dhr1 interaction

Because the mutations that suppressed *bud23*Δ mapped within the region that we identified as important for interaction with Dhr1, Margarida Anjos tested if they affected interaction using yeast two-hybrid studies. Although the individual point mutants and combined Utp14$_{multi\text{-}sup}$ mutant had no obvious effect on Dhr1 interaction (Figure 3.9 and data not shown), Utp14$_{multi\text{-}Ala}$ and Utp14$_{\Delta 719\text{-}780}$ displayed increasing loss of interaction (Figure 3.9) that correlated with their reduced ability to complement loss of Utp14 (Figure 3.8B). These results suggest that the motif identified by mutations that suppress *bud23*Δ contributes to interaction with Dhr1.

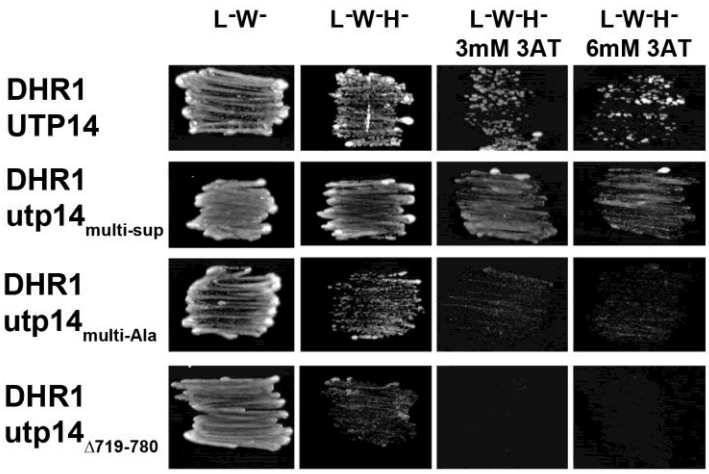

Figure 3.9Utp14 mutants and Dhr1 interaction by yeast two-hybrid

Combining suppressing mutations, multiple alanine substitutions or deletion of the region of Utp14 identified by suppressing mutations causes an increasing defect in Dhr1 interaction scored by two-hybrid assay.

3.5 rRNA processing in utp14 mutants

Cleavage at site A2 produces 20S and 27SA2 pre-rRNAs (Figure 3.10A) and is the primary event that separates the RNAs of the pre-40S subunit from the pre-60S subunit. We previously showed that deletion of *BUD23*, loss of *UTP14,* or a catalytically inactive *dhr1* mutant results in loss of the 27SA2 pre-rRNA intermediate (21, 26, 27), indicating either a failure in A2 cleavage or a delay in A2 cleavage such that cleavage at A3 precedes cleavage at A2. I compared pre-rRNA processing in WT and *utp14* mutant cells. As we have shown previously, WT cells displayed a strong signal for 27SA2 pre-rRNA, which was absent from Utp14-depleted cells (Figure 3.10B, lane 1). $Utp14_{multi\text{-}Ala}$, $Utp14_{multi\text{-}sup}$ and $Utp14_{\Delta 719\text{-}708}$ cells contained decreasing amounts of 27SA2 RNA indicating an increasingly severe defect in cleavage at A2 (Figure 3.10B, lanes 3-5). The mutants also showed an increase in 35S and a modest increase in 23S RNA (Figure 3.10C, lanes 3-5), which results from cleavage at A3 without earlier cleavages at A0, A1 or A2. I also detected low levels of 21S, which increased with the severity of the growth defect of the mutant (Figure 3.10B, lanes 3-5). 21S results from correct processing at A0 and A1 to generate the mature 5'-end of 18S but is cleaved at A3 rather than A2 on the 3'-end. Despite the absence of cleavage at A2, 20S levels were not significantly altered. This is consistent with the notion that A2 cleavage occurs after A3 cleavage in these mutants. A similar phenotype of loss of 27A2 but not 20S pre-rRNA was seen for *bud23*Δ cells (26). These results suggest that the $Utp14_{multi\text{-}Ala}$, $Utp14_{multi\text{-}sup}$ and $Utp14_{\Delta 719\text{-}708}$ mutants are hypomorphic alleles of *UTP14* with defects intermediate between WT and complete loss of Utp14 function. The

loss of 27SA2 in these *utp14* mutants was not due to loss of Utp14 protein, as these proteins were readily detected by western blotting (Figure 3.11). Rather, loss of 27SA2 must be due to a specific defect in the function of the mutant Utp14 proteins.

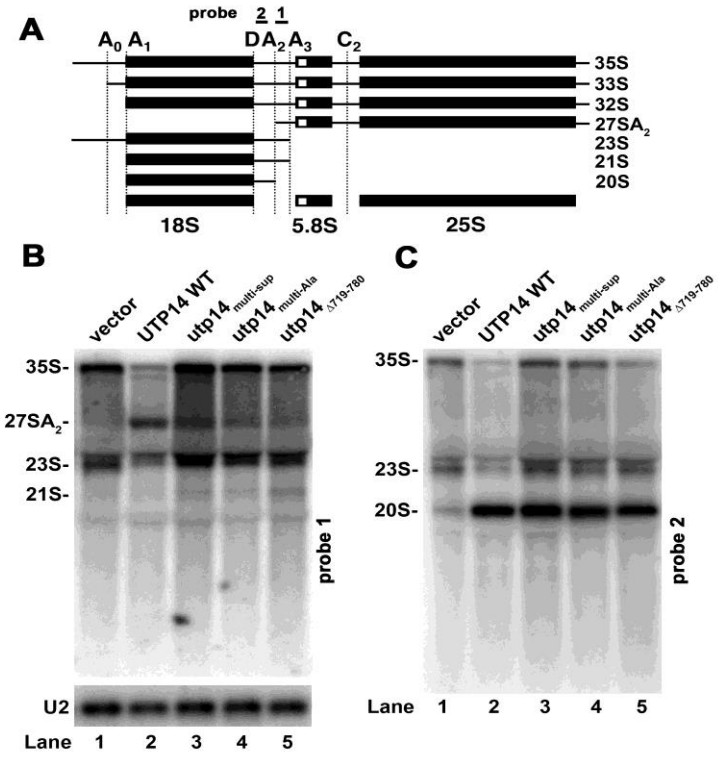

Figure 3.10 Utp14 mutants show reduced 27SA2 pre-rRNA.

(A) Cartoon for ribosomal RNA processing. (B and C) Northern blots:P_{GAL1}-Utp14 (AJY3243) containing empty vector (pAJ100) (lane 1), wild-type *UTP14* (pAJ1919) (lane 2), utp14multi-Sup(pAJ3264) (lane 3), utp14multi-Ala(pAJ3276) (lane 4),and utp14Δ719-780 (pAJ3276) (lane 5) were grown in SD Ura- galactose medium and then shifted to SD Ura- glucose medium for 6 h at 30°C. All cultures were harvested at an OD600 of 0.3. Total RNA was extracted using hot-phenol, separated on a 1% agarose–formaldehyde denaturing gel, transferred to a membrane, and probed with (B) probe 1 (AJO603, site A2-A3) and (C) probe 2 (AJO130, site D-A2). U2 RNA (probed with AJO962) was used as a loading control.

3.6 Impaired function of Utp14 phenocopies a Dhr1 catalytic mutant

I reasoned that Utp14 mutants with reduced interaction with Dhr1 should inhibit recruitment of Dhr1 to the pre-ribosome. To explore this idea I examined the sedimentation of Dhr1 in sucrose gradients in the presence of WT or mutant Utp14. WT and mutant Utp14 were expressed in cells in which genomic Utp14 was under the control of the glucose-repressible *GAL1* promoter. In the presence of WT Utp14, Dhr1 sedimented primarily as free protein at the top of the gradient (Figure 3.11A, fractions 1, 2). However, in the presence of each of the three utp14 mutants, I observed a shift in the sedimentation of Dhr1 from the top of the gradient to ~55S (Figure 3.11B-D, fractions 5, 6). The effect was greater for $Utp14_{multi\text{-}Ala}$ than for $Utp14_{multi\text{-}sup}$, correlating with their severity of impact on function. Clearly, mutant Utp14 did not prevent recruitment of Dhr1 to the pre-ribosome. Rather, the data suggest that mutant Utp14 caused the accumulation of wild-type Dhr1 in the pre-ribosome. Evidently, the function of Utp14 is more than merely binding to and recruiting Dhr1. The accumulation of Dhr1 was somewhat less pronounced for $Utp14_{\Delta 719\text{-}780}$ despite its more severe growth defect. We suspect this mutant is partially defective in recruitment of Dhr1 in addition to failing to activate Dhr1 (see below).

We previously showed that mutant $Dhr1_{K420A}$, which is defective for ATP binding and hydrolysis, arrests SSU maturation by trapping a U3 bound ~55S particle that also contains the U3 associated proteins Mpp10 and Imp4 (21). Therefore, I monitored the sedimentation of U3, Mpp10 and Imp4 in the presence of the Utp14 mutants. Indeed, these trans-acting factors also shifted in distribution with a significant fraction shifting from the

90S region (Figure 3.11A-D, fractions 9, 10) to cosediment with Dhr1 at ~55S (Figure 3.11A-D, fraction 5-6). To confirm that the co-sedimentation of Dhr1 with mutant Utp14 and U3 (Figure 3.11) reflected association with a pre-40S particle, Immunoprecipitated WT Utp14 or Utp14$_{multi\text{-}Ala}$ and probed for the presence of Dhr1, Imp4, Mpp10, U3 and pre-rRNAs. I observed an accumulation of Dhr1, Imp4 and Mpp10 in the Utp14$_{multi\text{-}Ala}$ sample compared to WT Utp14 (Figure 3.12A, compare lanes 3 and 4), demonstrating that these proteins accumulate in a common complex. I also observed a striking accumulation of 20S pre-rRNA as well as U3 in the Utp14$_{multi\text{-}Ala}$sample compared to WT (Figure 3.12B, compare lanes 3 and 4). However, I did not detect accumulation of 21S (Figure 3.12C). The lack of 27SA2 product (Figure 3.10 B, lane 4) and accumulation of 20S pre-rRNA in the Utp14 particle, could be explained if A2 cleavage is delayed relative to A3 cleavage in the Utp14$_{multi\text{-}Ala}$ mutant, so that 21S pre-rRNA is processed into 20S in the stalled particle, as we suggested for the catalytic *dhr1* mutant *dhr1*$_{K420A}$ (21). Alternatively, a failure to recycle U3 from the stalled mutant Utp14 particle would also lead to reduction in U3-dependent cleavages at A0, A1 and A2. The relative contributions to pre-rRNA processing of delayed cleavage at A2 and the consequences of failing to recycle U3 remain to be determined. I conclude that the altered sedimentation of Dhr1, U3, Imp4, Mpp10 and Utp14 is due to accumulation of these factors on a stalled pre-40S particle. The similarity in phenotype between the *utp14* mutants and the catalytic *dhr1*$_{K420A}$ mutant led us to posit that Utp14 activates Dhr1 helicase activity.

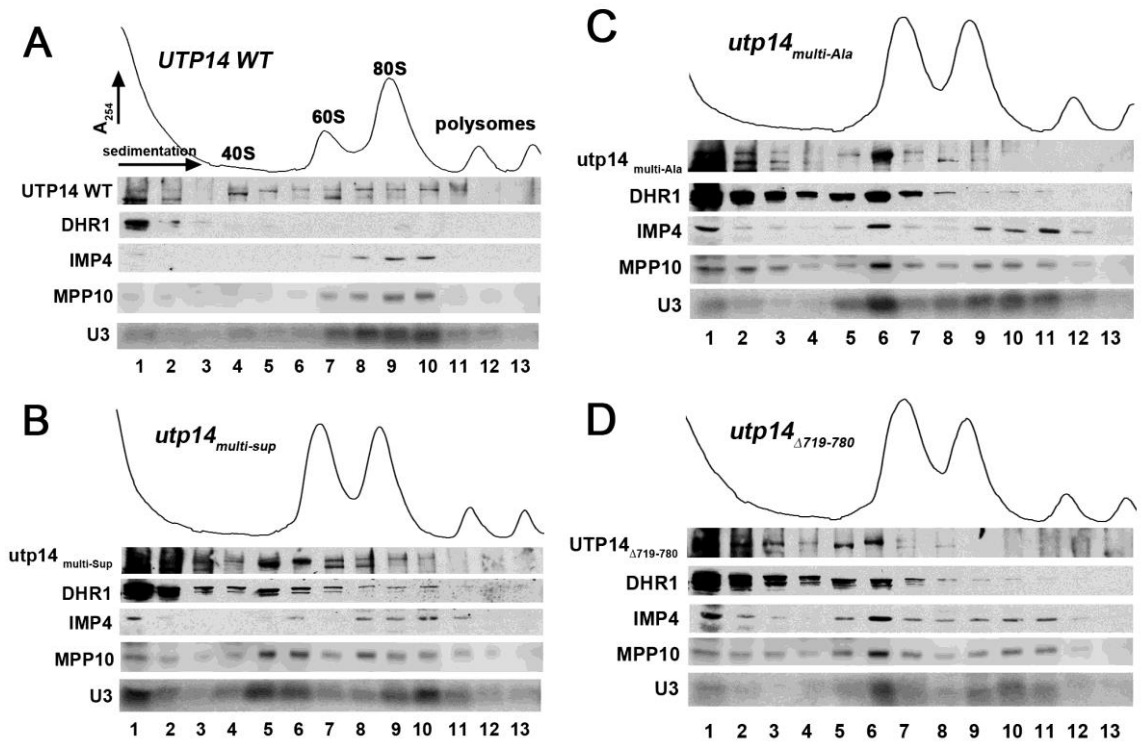

Figure3.11. Dhr1 sedimentation in *utp14* mutants

Whole-cell extracts were prepared from a PGAL1-UTP14 strain (AJY3243) containing plasmids expressing (A) wild-type *UTP14* (pAJ3308), (B) utp14multi-Sup(pAJ3309), (C) utp14multi-Ala (pAJ3313), and (D) utp14Δ719-780 (pAJ3310) grown in glucose medium for 6 h. Extracts were subjected to sucrose density gradient ultracentrifugation. Proteins were precipitated from fractions and subjected to western blotting and RNA was extracted and subjected to northern blotting. Utp14, Dhr1, Imp4 and Mpp10 were detected using anti-GFP (Utp14), anti-myc (Dhr1), anti-Imp4, and anti-Mpp10 antibodies, respectively. U3 was probed with AJO2194.

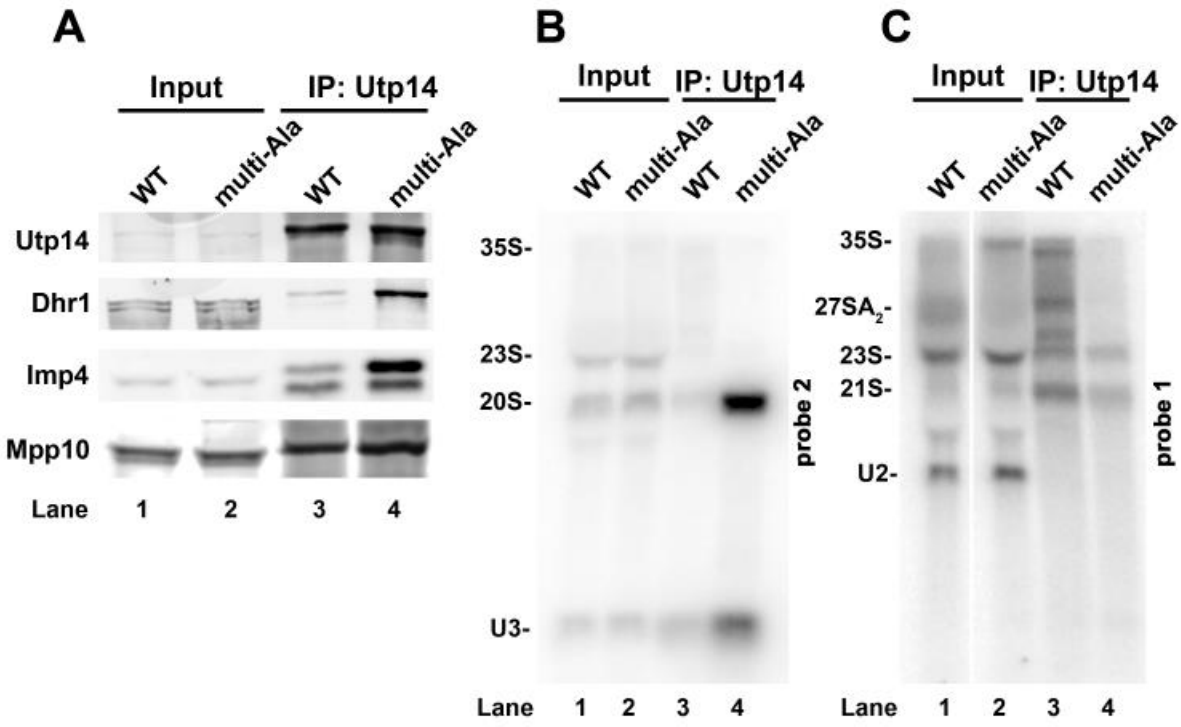

Figure 3.12 Utp14$_{multi\text{-}Ala}$ coimmunoprecipitates a pre-40S particle containing U3 and Dhr1.

(A) Utp14 WT and the multi-alanine mutant were immunoprecipitated from extracts prepared from strains as described in Figure 3.11 Immunoprecipitated proteins were analyzed by SDS-PAGE and western blotting for Utp14, Dhr1, Imp4 and Mpp10. The asterisk indicates a probable proteolytic product of Imp4.(B, C) RNAs were extracted from the immunoprecipitated samples and analyzed by northern blotting with probe1 to detect pre-rRNAs containing the D-A2 fragment (B) and probe 2 to detect pre-rRNAs containing the A2-A3 fragment (C), as described in Figure 3.

3.7 Utp14 stimulates the unwinding activity but not the ATPase activity of Dhr1.

To assess whether Utp14 binds to and stimulates unwinding activity of Dhr1, Xin Liu, our collaborator, expressed and purified both proteins. Dhr1 was expressed with a C-terminal His6 tag in *Escherichia coli* and the recombinant protein was purified as described (21). Utp14, Utp14$_{\text{multi-Ala}}$ and Utp14$_{\Delta 719\text{-}780}$were expressed with a N-terminal His6 tag in *E. coli* and purified (Materials and Methods). I tested that Dhr1-His6 fully complemented a *dhr1* null mutant (21) and His6-Utp14 fully complemented the *utp14* null mutant in yeast (Figure 3.13). This result demonstrated that the tags did not interfere with the function of either protein *in vivo*.

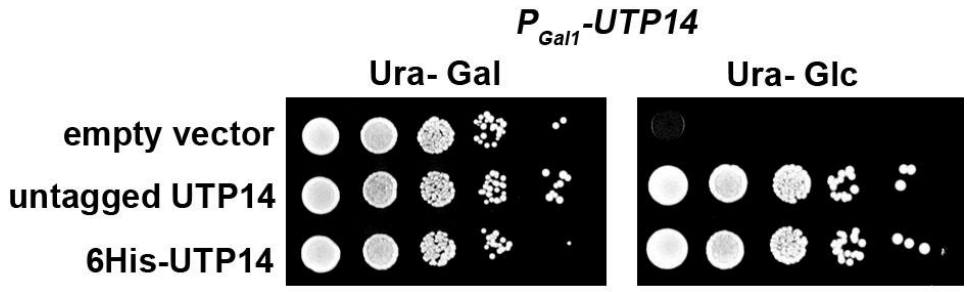

Figure 3.13 6xHis-UTP14 complements the function of UTP14.

Empty vector (pRS416), untagged UTP14 (pAJ1919) and 6xHis-UTP14 (pAJ3331) were transformed in PGal1-UTP14 strain (AJY3243) and grown on SD Ura- glucose medium and SD Ura- galactose for 3 days at 30°C.

To test if Utp14 stimulates unwinding activity of Dhr1, Xiu Liu used established assays with a substrate that mimics one of the three genetically verified U3-pre-rRNA duplexes: the U3-ETS2 duplex (21). The U3-ETS2 duplex comprises full-length U3

snoRNA bound to nts 281 to 291 of the 5'ETS of the pre-rRNA (Figure 3.14A) and is required for subsequent U3-pre-rRNA interactions *in vivo*(20). This duplex forms spontaneously and is stable *in vitro* (41). The U3-ETS2 duplex unwinding reactions were performed under pre-steady state conditions with an excess of enzyme over the duplex substrate and low substrate concentrations to minimize duplex re-formation. To enhance detection of Utp14-dependent stimulation of Dhr1 unwinding activity, the enzyme concentration was lowered to the point where unwinding activity by Dhr1 alone was barely detectable (Figure 3.14B, lane 4). Addition of Utp14 to a reaction containing Dhr1 resulted in a noteworthy increase in unwinding activity that was dependent on$ATP•Mg^{2+}$ (Figure 3.14B, compare lanes 4, 5 and 6). No activity was observed with Utp14 alone in the presence of $ATP•Mg^{2+}$ (Figure 3.14B, lane 8), indicating that this protein has no intrinsic helicase activity. Stimulation of Dhr1-dependent unwinding by Utp14 was also seen when both proteins were 500 nM, although the fold stimulation was reduced (data not shown). Compared with Utp14, $Utp14_{multi\text{-}Ala}$ and the $Utp14_{\Delta 719\text{-}780}$ showed reduced activity (Figure 3.14B, compare lane 6 with lanes 9 and 10). To quantitate these activities, he performed time course assays and fit the data to determine the unwinding (k_{unw}) rate constant as described in (42). Addition of WT Utp14 to the Dhr1 reactions stimulated k_{unw} by 98-fold, whereas the mutants showed less stimulation. Addition of $Utp14_{multi\text{-}Ala}$ and of $Utp14_{\Delta 719\text{-}780}$ to the Dhr1 reactions stimulated the k_{unw} by 41-fold and 18-fold, respectively, in accord with the reduced function of these mutants *in vivo* (Figure 3.9 and 3.10).

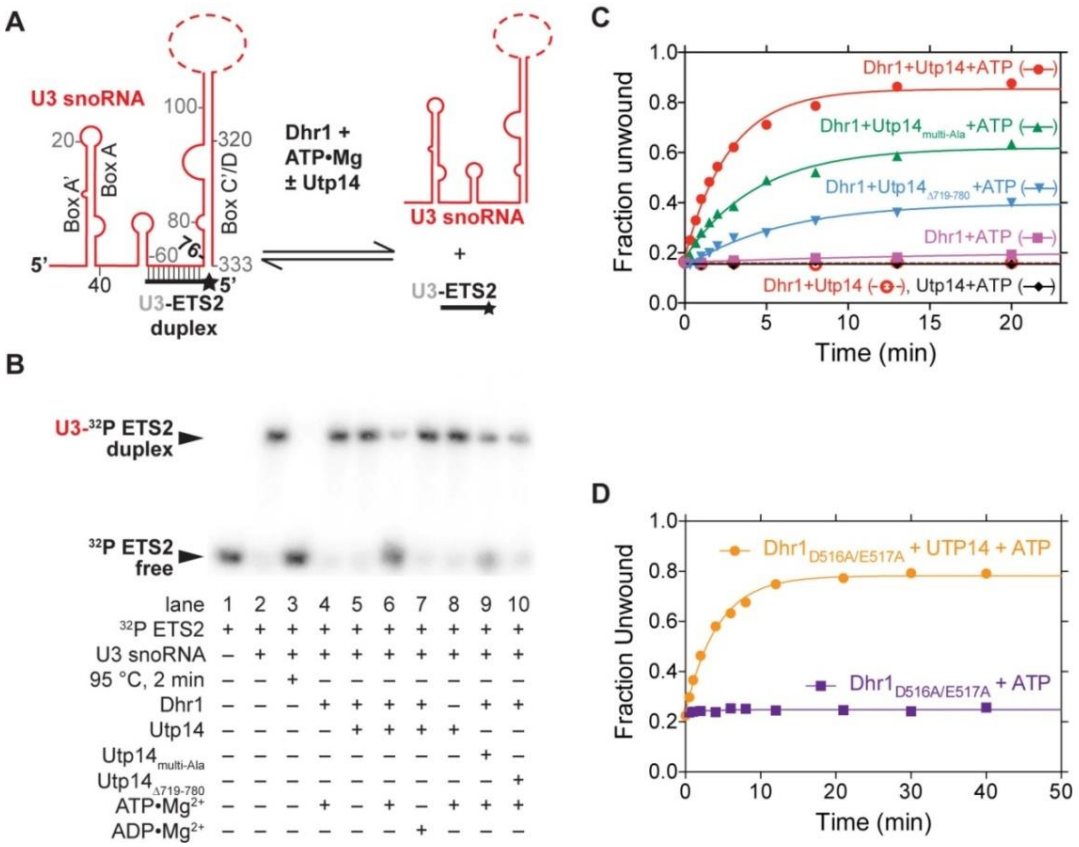

Figure 3.14 Utp14 activates Dhr1 unwinding activity in vitro.

(A) Cartoon of U3-ETS2 substrate used for unwinding assays. Full length U3 snoRNA was used for the reactions in (B and C). (B) Representative unwinding reactions stopped after 20 min. EMSAs separated the ^{32}P-labeled ETS2 free (unwound) from its duplex form. The RT reaction contained 50 nM Dhr1 (WT or mutant), 200 nM Utp14 (WT or mutant), 1 mM ATP, ≤0.3 nM U3-ETS2 duplex with other reagents described in Materials and Methods. (C)Fraction unwound was plotted as a function of time after addition of:ATP and either Utp14 (black diamonds); Dhr1 (purple squares); Dhr1 in the presence of either Utp14 (red squares), Utp14Multi-Ala (green triangles), Utp14Δ719-780 (blue reverse triangles); or Dhr1 and Utp14 in the absence of ATP (red circles). (D) Fraction unwound was plotted as a function of time after addition of ATP and Dhr1D516A/E517A in the absence (purple squares) or presence of Utp14 (orange circles).

Previously, we established that Dhr1 shares mechanistic similarities with DEAD box helicases in that unwinding requires ATP binding but not hydrolysis whereas product recycling requires ATP hydrolysis (21). To explore whether Utp14 stimulates Dhr1-dependent unwinding, we tested the activity of the $Dhr1_{D516A/E517A}$ mutant, which eliminates the catalytic and metal binding carboxylates and thus probes the unwinding and not the recycling step (21). Utp14 stimulated the k_{unw} of $Dhr1_{D516A/E517A}$ by 26-fold (Figure 3.14D), which is less than 96-fold stimulation observed for WT Dhr1 (Figure 3.14C). Thus, Utp14 accelerates the Dhr1-dependent unwinding step; however, because Utp14 stimulated WT Dhr1 to a greater extent than $Dhr1_{D516A/E517A}$, Utp14 must also contribute to other steps, such as substrate recruitment and/or product recycling.

DEAH helicases are often activated by G-patch proteins that stimulate both unwinding and ATPase activity. To examine whether Utp14 shares these properties, we first analyzed sequence conservation within the Utp14 family. G-patch proteins are defined by a consensus sequence: *hhx*(3)G*ax*(2)G*x*G*h*G*x*(4)G where *a* is an aromatic residue, *h* is hydrophobic, and *x* can be any amino acid (24). Whereas many positions allow some divergence from this sequence the first glycine followed by an aromatic residue are invariant. Utp14 proteins contain a highly glycine-rich conserved motif, hPGWGxWxG*x*G. Even though the dipeptide GW is invariant, the larger motif does not fit the consensus of a G-patch protein. Dhr1 has RNA-stimulated ATPase activity (21). Consequently, Xin Liu tested whether Utp14 could stimulate the ATPase activity of Dhr1 like other G-patch proteins that activate the ATPase activities of helicases. The ATPase activity of Dhr1 was

indistinguishable in the presence or absence of Utp14, regardless of the presence or absence of poly(A) (Figure 3.15). Furthermore, Utp14 alone showed no intrinsic ATPase activity in contrast to its annotation as an ATPase (43). These results indicate that Utp14 stimulates Dhr1 unwinding activity without increasing its RNA-dependent ATPase activity. Thus, we conclude that Utp14 is not a G-patch protein or represents a divergent class of G-patch proteins.

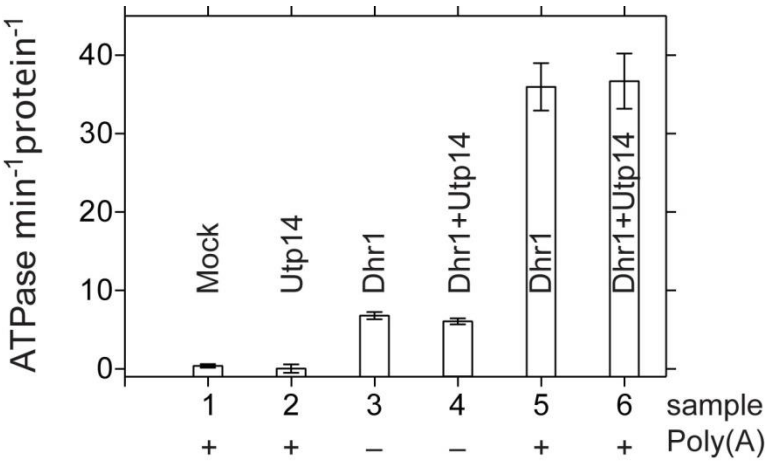

Figure 3.15 Utp14 does not stimulate the ATPase activity of Dhr1.

Initial velocities of Pi released after addition of 1 mM ATP at room temperature in the presence or absence of the poly(A)added to either Dhr1, Dhr1 with Utp14, Utp14, or mock with other reagents described in Materials and Methods. Each protein had a final concentration of 0.5 μM. In the activity units of $min^{-1}protein^{-1}$, protein refers to either Dhr1, Utp14 or the complex of the two. Similar results were obtained at 50 nM Dhr1 in the presence or absence of 200 nM Utp14 (Fig. S5) or at lower poly(A) concentration (data not shown).

3.8 Dhr1 and Utp14 form a complex in vitro

To determine the stoichiometry of the Dhr1:Utp14 complex, Xiu Liu performed crosslinking assays with BS^3, a reagent that reacts with surface lysine residues, and used mass spectrometry to probe its stoichiometry (Materials and Methods). Crosslinking slightly altered migration of the individual proteins on SDS-PAGE (Figure 3.16A, compare lanes 8 to 11 with lanes 1 and 4). When both proteins were present, a slower migrating band was observed, correlating with loss of the individual protein bands (Figure 3.16A, compare lanes 5-7 with lanes 1-4), consistent with a Dhr1:Utp14 complex. Interestingly, neither $Utp14_{multi\text{-}Ala}$ nor $Utp14_{\Delta 719\text{-}780}$ produced as much of the higher order crosslinked species with Dhr1 as was observed with WT Utp14 and Dhr1 (Figure 3.16A, compare lane 5 with lanes 6 and 7). Mass spectrometry verified that individual proteins modified by BS^3 showed increased mass: 166 kDa for Dhr1 and 122 kDa for Utp14. A heavier species was observed at 287 kDa only in the presence of both proteins, which was consistent with a 1:1 stoichiometry of Dhr1:Utp14 (Figure 3.16B, compare red trace with black and blue traces). The low intensity of this 287 kDa species likely arose from the inefficiency of ionizing such a large complex. Together these results provide evidence that Dhr1 and Upt14 form a 1:1 complex and that both Utp14 mutants weaken this interaction in accord with the two-hybrid data (Figure 3.9). Whereas a 1:1 complex is observed, technical limitation of SELDI-TOF mass spectrometry cannot rule out the presence of higher order complexes as well.

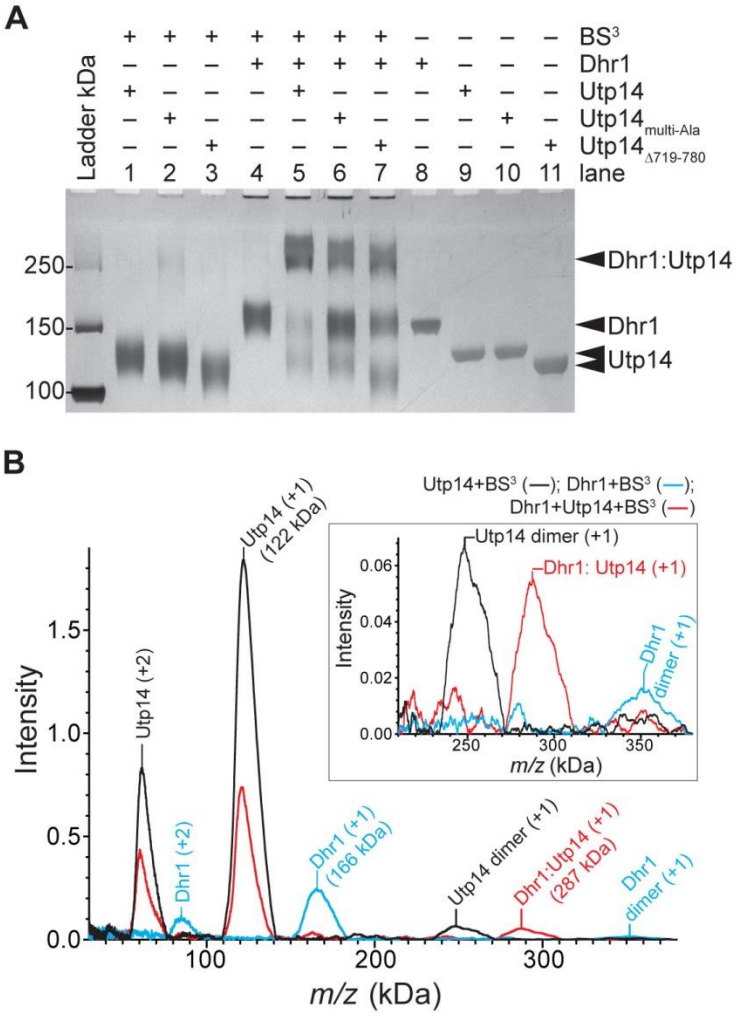

Figure 3.16 Dhr1 and Utp14 form 1:1 complex in vitro.

(A) Representative cross-linking reactions stopped after 30 min. SDS-PAGE separated the cross-linked protein complex from individual protein. The RT reaction contained 2 μM of each protein with other reagents described in Materials and Methods. (B) Mass spectrometry analysis of the same sample of lane 1 (Utp14, black trace), lane 4 (Dhr1, blue trace) and lane 5 (both proteins, red trace) in panel A. Mass of the individual proteins, Dhr1 (166 kDa) and Utp14 (122 kDa), have increased by more than 10% due to modification of the large number of lysine resides in each protein: 123 and 99, respectively. Upon addition of both proteins (red trace) a new mass appears, 287 kDa, consistent with formation of a 1:1 complex. The upper right inset shows an enlargement of the intensity of the masses centered around 300 kDa.

3.9 Utp14and Bud23 together are required for efficient association of Dhr1 with the pre-ribosome

A major question is how is Dhr1 recruited to and activated at the appropriate time during SSU biogenesis. To address this question I investigated whether Utp14 recruits Dhr1 to the pre-ribosome. Because WT Dhr1 does not stably associate with pre-ribosomes, I used the $Dhr1_{K420A}$ mutant that does stably interact with a ~55S pre-ribosomal particle ((21) and Figure 3.17A, fraction 6). We previously showed that Bud23 binds to the N-terminal domain of Dhr1 and that mutations in Dhr1 partially suppress the growth defect of *bud23*Δ cells (28). Despite the physical and functional interaction between Bud23 and Dhr1, loss of Bud23 has no observed effect on the sedimentation of $Dhr1_{K420A}$ ((28) and Fig. 8B). This suggests that Bud23 alone is not necessary for recruitment of Dhr1 to the pre-ribosome, contrary to a recent report (25). Given that Utp14 also interacts with Dhr1, I asked if Utp14 was required for association of Dhr1 with the pre-ribosome. Again, I did not observe any obvious change in the sedimentation of $Dhr1_{K420A}$ in the absence of Utp14 (Figure 3.17C). However, when we eliminated both Utp14 and Bud23 by depleting Utp14 from Bud23-deficient cells, we saw a significant loss of $Dhr1_{K420A}$from the ~55S region of the gradient (Figure 3.17D, fractions 5, 6) and corresponding accumulation of free protein at the top of the gradient (Figure 3.17D, fractions 1, 2). These findings suggest that efficient association of Dhr1 with the pre-ribosome requires both Bud23 and Utp14.

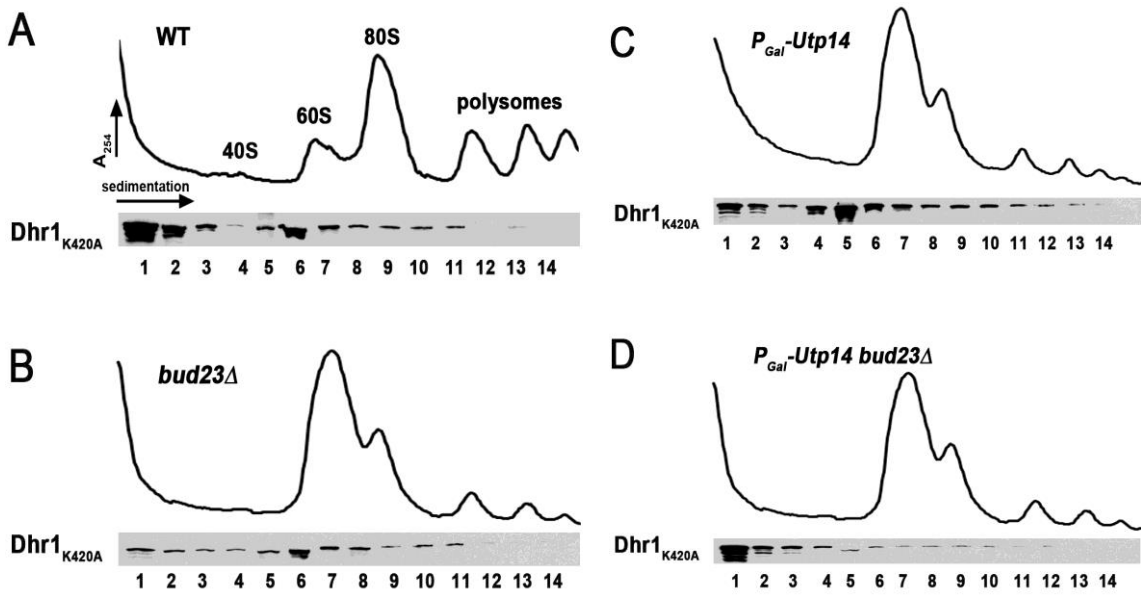

Figure 3.17 Utp14 and Bud23 together are necessary for efficient Dhr1 recruitment to the pre-ribosome.

Plasmid pAJ3081(dhr1K420A-13myc) was transformed into (A) Wild Type (BY4741), (B) bud23Δ(AJY2161), (C)PGAL1-Utp14(AJY3243), and (D) PGAL1-Utp14 bud23Δ (AJY3245) strains. Whole-cell extracts from strains grown in Leu- galactose that were shifted to Leu- glucose medium for 6 h, were subjected to sucrose density gradient ultracentrifugation. Proteins were precipitated from fractions and subjected to western blotting. Dhr1K420A was detected with anti-myc antibody.

Chapter 4 Discussion and Future Direction[4]

My results identify Utp14 as an essential factor required for activating the DEAH/RHA helicase Dhr1, which removes U3 from the pre-ribosome to allow folding the CPK. In addition to activating Dhr1, Utp14 is also required for recruiting Dhr1 to the pre-ribosome. I conclude this based on the result that both Utp14 and the RNA methyltransferase Bud23 are required for stable association of Dhr1 with the pre-ribosome. Thus, Utp14 has two functions: together with Bud23 it recruits Dhr1 to the pre-ribosome and it activates Dhr1 in the context of the pre-ribosome.

I uncovered the connection between Utp14 and Dhr1 because mutations in either protein suppress the growth and ribosome biogenesis defects of a *bud23*Δ mutant (27, 28). In earlier work we showed that the *utp14-A758G* mutation partially suppressed the growth defect of *bud23*Δ. Here, we found that additional mutations that suppress *bud23*Δ map to a short segment of Utp14 necessary for stimulation of Dhr1 unwinding activity and my results suggest that this is through direct physical interaction with Dhr1.

BUD23, *DHR1* and *UTP14* are each needed for efficient cleavage at A2. Interestingly, whereas the single point mutation *utp14-A758G* suppresses the A2 cleavage defect of *bud23*Δ cells, simultaneous mutation of multiple residues in Utp14 eliminated suppression and resulted in an A2 cleavage defect. Apparently, subtle perturbation of the

[4]Chapter 4 is mainly based on previously published article: Zhu J, Liu X, Anjos M, Correll CC, Johnson AW. Utp14 Recruits and Activates the RNA Helicase Dhr1 To Undock U3 snoRNA from the Preribosome. Mol Cell Biol. 2016;36(6):965-78. PMCID: 4810474. I contributed to the whole chapter 4.

function of this peptide suppresses *bud23*Δ whereas more severe perturbation leads to loss of function. What then is the function of Bud23 and how do mutations in Utp14 suppress *bud23*Δ? Since mutations in Utp14 reduce the activity of Dhr1 and suppress *bud23*Δ, one possibility is that Bud23 slows or limits the activity of Dhr1. Bud23 and Utp14 are both needed for stable association of Dhr1 with the pre-ribosome. Perhaps in the absence of Bud23, ATP hydrolysis by Dhr1 leads to unproductive events and premature release of Dhr1. Thus, mutations that slow its activity could allow more time for productive engagement with its substrate. This thinking is analogous to what has been proposed for Prp5, a DEAD box helicase required for spliceosome assembly. Mutations in Prp5 that reduce its intrinsic ATPase activity increased the fidelity of splicing a suboptimal intron (44). Alternatively, Bud23 may stabilize an RNA structure in the pre-ribosome, consistent with the fact that Bud23 protein, but not its methyltransferase activity, is important for supporting ribosome assembly (26). Dhr1 action on a destabilized pre-40S may lead to mis-folding or mis-assembly that is recognized by surveillance systems, triggering discard of the subunit. Reducing the rate of Dhr1 unwinding could allow sufficient time for productive RNA-RNA or RNA-protein rearrangements in the absence of Bud23.

The results presented in this work provide a compelling evidence for Utp14 regulation of Dhr1 helicase function in small subunit biogenesis. However, there are still some key unanswered questions that need to be addressed.

4. 1 How is Utp14 recruited to the pre-ribosome at the appropriate time in SSU biogenesis?

Utp14 was initially characterized as a component of the SSU Processome(9) and likely associates with the pre-ribosome before Bud23(27). Bud23 methylates G1575 in the 3'-major head domain of the subunit (25, 26) and presumably binds to its RNA target site only after it is properly folded but before A2 cleavage, as *bud23*Δ mutants are defective for cleavage at this site (26). Both Utp14 and Bud23 remain associated with the subunit after A2 cleavage (27) and thus mark the transition from the 90S particle to the pre-40S particle. As most RNA helicases typically lack substrate specificity and need auxiliary factors for substrate recognition, and both Bud23 and Utp14 are needed for stable association of Dhr1 with the pre-ribosome, I suggest that these two proteins, together, couple Dhr1 activity to the status of rRNA transcription and folding within the pre-ribosome. Thus, Utp14 must bind to the pre-ribosome earlier than or with Dhr1.

It has recently been reported that Utp14 binds to the pre-ribosome only after completion of transcription of the 3' minor domain of 18S rRNA (45). It is possible that Utp14 binding to the 3'-minor domain would provide a mechanism to ensure that Dhr1 is activated to remove U3 only after the entire 18S rRNA is transcribed.

Since I found Utp14 is an RNA binding protein (unpublished data), a question is raised: is Utp14 recruited directly to a particular RNA sequence that needs only to be transcribed, or to an RNA structure that would require folding and possibly proteins to promote folding? In order to address this question, the Utp14 binding sites of pre-rRNA

could be identified by the UV cross-linking and analysis of cDNA (CRAC) method. The CRAC data will be confirmed by yeast three-hybrid assay and by testing if Utp14 loses interaction with pre-rRNA when mutating the specific nucleotides of pre-RNA.

4.2 How does Utp14 activate Dhr1 to release U3 at the appropriate time in ribosome assembly?

Base-pairing between U3 and the pre-rRNA orchestrates early RNA folding and cleavage events. However, these early events, leading to the cleavage at A2, occur very rapidly; in actively growing yeast, cleavage at A2 occurs within 50s of initiation of transcription (46). Thus, the binding and release of U3 is highly dynamic and must be driven by factors, such as Imp3, which promotes its annealing with pre-rRNA (41) and Dhr1, which promotes its dissociation (21). Whereas cleavage at A0, A1 and A2 are all U3-dependent, these three cleavage sites appear to separate into two functionally distinct groups. Production of the mature 5' end of 18S by A0 and A1 cleavage requires U3 docking, whereas efficient A2 cleavage is expected to require undocking of U3. Thus U3 docking produces the 5' end of 18S whereas U3 release signals SSU biogenesis by liberating the SSU 20S precursor from the pre-rRNA. In this model U3 docking and undocking provide distinct structural switches to mark steps during SSU biogenesis.

Various DEAH/RHA RNA helicases depend on G-patch proteins for their recognition of substrates and for their activation (24). Here, we have shown that Utp14 binds to and activates Dhr1 but neither possesses the canonical G-patch sequence nor stimulates ATPase activity upon activation of unwinding activity, two hallmarks of known

G-patch proteins that activate RNA helicases. In contrast, we found that Utp14 stimulated the helicase activity of Dhr1 without stimulating its ATPase activity. Such stimulation of unwinding without activation of ATPase activity is not without precedent. The Ski2-like RNA helicase Brr2 is required for pre-mRNA splicing and its unwinding activity can be stimulated by Prp8, which also reduces its ATPase activity (47). In this case, Prp8 increases the coupling between ATP hydrolysis and productive unwinding by Brr2 (48) by a mechanism that is unclear. Utp14 also appears to increase the coupling between ATP hydrolysis and productive unwinding by Dhr1, because the presence of Utp14 stimulates unwinding activity by Dhr1 without affecting rates of hydrolysis.

A possible molecular basis of such stimulation is provided by the DNA helicase PcrAin which its activator RepD stimulates the unwinding PcrA without affecting ATPase activity (49, 50). RepD exploits a common feature of the reaction cycle of helicases with tandem RecA-like domains—these domains cycle between an open, inactive conformation and a closed, active conformation (51). In the active form the two RecA-like domains come together to form the NTP and RNA duplex binding cleft. Cross-linking and FRET studies suggest that RepD stimulates the helicase activity of PcrA by locking the tandem RecA-like domains in an active closed conformation (39) and this is accomplished without stimulated ATPase activity (49). Perhaps Utp14 binding to Dhr1 similarly stabilizes a closed conformation of the RecA-like domains of Dhr1 to couple unwinding to ATPase activity.

However, because Utp14 is an RNA binding protein, it is currently not easy to distinguish between roles in substrate recruitment and catalytic activation of Dhr1. This could be addressed if Utp14 could be separated into functional domains that separately bind RNA and activate Dhr1. In my unpublished data, I found that $Utp14_{1\text{-}265}$ but not $Utp14_{707\text{-}899}$ binds to the pre-ribosome. As I have presented that $Utp14_{multi\text{-}Ala}$ and $Utp14_{\Delta 719\text{-}780}$ have reduced activation of Dhr1 unwinding activity, it implies that the peptides for activating Dhr1 helicase function locate in $Utp14_{707\text{-}899}$. These preliminary results suggest that Utp14 can be separated into pre-ribosome binding and Dhr1 activating domains. It will be of interest to express and purify these domains and test them *in vitro* assays for RNA binding and Dhr1 activation. The identification of a domain that lacks RNA binding but retains Dhr1 binding would allow us to separate the contributions of Utp14 to substrate recruitment and catalytic activation of Dhr1.

Bibliography

1. Wilson DN, Doudna Cate JH. The structure and function of the eukaryotic ribosome. Cold Spring Harb Perspect Biol. 2012;4(5). PMCID: 3331703.
2. Ramakrishnan V. Ribosome structure and the mechanism of translation. Cell. 2002;108(4):557-72.
3. Henras AK, Plisson-Chastang C, O'Donohue MF, Chakraborty A, Gleizes PE. An overview of pre-ribosomal RNA processing in eukaryotes. Wiley Interdiscip Rev RNA. 2015;6(2):225-42. PMCID: 4361047.
4. Mougey EB, O'Reilly M, Osheim Y, Miller OL, Jr., Beyer A, Sollner-Webb B. The terminal balls characteristic of eukaryotic rRNA transcription units in chromatin spreads are rRNA processing complexes. Genes Dev. 1993;7(8):1609-19.
5. Bernstein KA, Gallagher JE, Mitchell BM, Granneman S, Baserga SJ. The small-subunit processome is a ribosome assembly intermediate. Eukaryot Cell. 2004;3(6):1619-26. PMCID: 539036.
6. Henras AK, Soudet J, Gerus M, Lebaron S, Caizergues-Ferrer M, Mougin A, et al. The post-transcriptional steps of eukaryotic ribosome biogenesis. Cell Mol Life Sci. 2008;65(15):2334-59.
7. Lamanna AC, Karbstein K. Nob1 binds the single-stranded cleavage site D at the 3'-end of 18S rRNA with its PIN domain. Proc Natl Acad Sci U S A. 2009;106(34):14259-64. PMCID: 2732849.
8. Oeffinger M, Fatica A, Rout MP, Tollervey D. Yeast Rrp14p is required for ribosomal subunit synthesis and for correct positioning of the mitotic spindle during mitosis. Nucleic Acids Res. 2007;35(4):1354-66. PMCID: 1849896.
9. Dragon F, Gallagher JE, Compagnone-Post PA, Mitchell BM, Porwancher KA, Wehner KA, et al. A large nucleolar U3 ribonucleoprotein required for 18S ribosomal RNA biogenesis. Nature. 2002;417(6892):967-70.
10. Krogan NJ, Peng WT, Cagney G, Robinson MD, Haw R, Zhong G, et al. High-definition macromolecular composition of yeast RNA-processing complexes. Mol Cell. 2004;13(2):225-39.
11. Perez-Fernandez J, Roman A, De Las Rivas J, Bustelo XR, Dosil M. The 90S preribosome is a multimodular structure that is assembled through a hierarchical mechanism. Mol Cell Biol. 2007;27(15):5414-29. PMCID: 1952102.
12. Beltrame M, Henry Y, Tollervey D. Mutational analysis of an essential binding site for the U3 snoRNA in the 5' external transcribed spacer of yeast pre-rRNA. Nucleic Acids Res. 1994;22(23):5139-47. PMCID: 523791.
13. Hodnett JL, Busch H. Isolation and characterization of uridylic acid-rich 7 S ribonucleic acid of rat liver nuclei. J Biol Chem. 1968;243(24):6334-42.
14. Hughes JM, Ares M, Jr. Depletion of U3 small nucleolar RNA inhibits cleavage in the 5' external transcribed spacer of yeast pre-ribosomal RNA and impairs formation of 18S ribosomal RNA. EMBO J. 1991;10(13):4231-9. PMCID: 453175.

15. Beltrame M, Tollervey D. Identification and functional analysis of two U3 binding sites on yeast pre-ribosomal RNA. EMBO J. 1992;11(4):1531-42. PMCID: 556602.
16. Hughes JM. Functional base-pairing interaction between highly conserved elements of U3 small nucleolar RNA and the small ribosomal subunit RNA. J Mol Biol. 1996;259(4):645-54.
17. Samarsky DA, Fournier MJ. Functional mapping of the U3 small nucleolar RNA from the yeast Saccharomyces cerevisiae. Mol Cell Biol. 1998;18(6):3431-44. PMCID: 108924.
18. Sharma K, Tollervey D. Base pairing between U3 small nucleolar RNA and the 5' end of 18S rRNA is required for pre-rRNA processing. Mol Cell Biol. 1999;19(9):6012-9. PMCID: 84488.
19. Beltrame M, Tollervey D. Base pairing between U3 and the pre-ribosomal RNA is required for 18S rRNA synthesis. EMBO J. 1995;14(17):4350-6. PMCID: 394519.
20. Dutca LM, Gallagher JE, Baserga SJ. The initial U3 snoRNA:pre-rRNA base pairing interaction required for pre-18S rRNA folding revealed by in vivo chemical probing. Nucleic Acids Res. 2011;39(12):5164-80. PMCID: 3130255.
21. Sardana R, Liu X, Granneman S, Zhu J, Gill M, Papoulas O, et al. The DEAH-box helicase Dhr1 dissociates U3 from the pre-rRNA to promote formation of the central pseudoknot. PLoS Biol. 2015;13(2):e1002083. PMCID: 4340053.
22. Colley A, Beggs JD, Tollervey D, Lafontaine DL. Dhr1p, a putative DEAH-box RNA helicase, is associated with the box C+D snoRNP U3. Mol Cell Biol. 2000;20(19):7238-46. PMCID: 86278.
23. Silverman E, Edwalds-Gilbert G, Lin RJ. DExD/H-box proteins and their partners: helping RNA helicases unwind. Gene. 2003;312:1-16.
24. Robert-Paganin J, Rety S, Leulliot N. Regulation of DEAH/RHA helicases by G-patch proteins. Biomed Res Int. 2015;2015:931857. PMCID: 4322301.
25. Letoquart J, Huvelle E, Wacheul L, Bourgeois G, Zorbas C, Graille M, et al. Structural and functional studies of Bud23-Trm112 reveal 18S rRNA N7-G1575 methylation occurs on late 40S precursor ribosomes. Proc Natl Acad Sci U S A. 2014;111(51):E5518-26. PMCID: 4280632.
26. White J, Li Z, Sardana R, Bujnicki JM, Marcotte EM, Johnson AW. Bud23 methylates G1575 of 18S rRNA and is required for efficient nuclear export of pre-40S subunits. Mol Cell Biol. 2008;28(10):3151-61.
27. Sardana R, White JP, Johnson AW. The rRNA methyltransferase Bud23 shows functional interaction with components of the SSU processome and RNase MRP. RNA. 2013;19(6):828-40. PMCID: 3683916.
28. Sardana R, Zhu J, Gill M, Johnson AW. Physical and functional interaction between the methyltransferase Bud23 and the essential DEAH-box RNA helicase Ecm16. Mol Cell Biol. 2014.
29. Sondalle SB, Baserga SJ. Human diseases of the SSU processome. Biochim Biophys Acta. 2014;1842(6):758-64. PMCID: 4058823.

30. Phipps KR, Charette J, Baserga SJ. The small subunit processome in ribosome biogenesis-progress and prospects. Wiley Interdiscip Rev RNA. 2011;2(1):1-21. PMCID: 3035417.
31. James P, Halladay J, Craig EA. Genomic libraries and a host strain designed for highly efficient two-hybrid selection in yeast. Genetics. 1996;144(4):1425-36. PMCID: 1207695.
32. SenGupta DJ, Zhang B, Kraemer B, Pochart P, Fields S, Wickens M. A three-hybrid system to detect RNA-protein interactions in vivo. Proc Natl Acad Sci U S A. 1996;93(16):8496-501. PMCID: 38700.
33. Longtine MS, McKenzie A, 3rd, Demarini DJ, Shah NG, Wach A, Brachat A, et al. Additional modules for versatile and economical PCR-based gene deletion and modification in Saccharomyces cerevisiae. Yeast. 1998;14(10):953-61.
34. Sardana R, Zhu J, Gill M, Johnson AW. Physical and functional interaction between the methyltransferase Bud23 and the essential DEAH-box RNA helicase Ecm16. Mol Cell Biol. 2014;34(12):2208-20. PMCID: 4054285.
35. Li Z, Lee I, Moradi E, Hung NJ, Johnson AW, Marcotte EM. Rational extension of the ribosome biogenesis pathway using network-guided genetics. PLoS Biol. 2009;7(10):e1000213.
36. Gerczei T, Correll CC. Imp3p and Imp4p mediate formation of essential U3-precursor rRNA (pre-rRNA) duplexes, possibly to recruit the small subunit processome to the pre-rRNA. Proc Natl Acad Sci U S A. 2004;101(43):15301-6. PMCID: 524450.
37. Gerczei T, Shah BN, Manzo AJ, Walter NG, Correll CC. RNA chaperones stimulate formation and yield of the U3 snoRNA-Pre-rRNA duplexes needed for eukaryotic ribosome biogenesis. J Mol Biol. 2009;390(5):991-1006. PMCID: 2881153.
38. He Y, Andersen GR, Nielsen KH. Structural basis for the function of DEAH helicases. EMBO Rep. 2010;11(3):180-6. PMCID: 2838688.
39. Walbott H, Mouffok S, Capeyrou R, Lebaron S, Humbert O, van Tilbeurgh H, et al. Prp43p contains a processive helicase structural architecture with a specific regulatory domain. EMBO J. 2010;29(13):2194-204. PMCID: 2905241.
40. Kelley LA, Mezulis S, Yates CM, Wass MN, Sternberg MJ. The Phyre2 web portal for protein modeling, prediction and analysis. Nat Protoc. 2015;10(6):845-58.
41. Shah BN, Liu X, Correll CC. Imp3 unfolds stem structures in pre-rRNA and U3 snoRNA to form a duplex essential for small subunit processing. RNA. 2013;19(10):1372-83. PMCID: 3854528.
42. Yang Q, Jankowsky E. ATP- and ADP-dependent modulation of RNA unwinding and strand annealing activities by the DEAD-box protein DED1. Biochemistry. 2005;44(41):13591-601.
43. Woolford JL, Jr., Baserga SJ. Ribosome biogenesis in the yeast Saccharomyces cerevisiae. Genetics. 2013;195(3):643-81. PMCID: 3813855.
44. Xu YZ, Query CC. Competition between the ATPase Prp5 and branch region-U2 snRNA pairing modulates the fidelity of spliceosome assembly. Mol Cell. 2007;28(5):838-49. PMCID: 2246091.

45. Chaker-Margot M, Hunziker M, Barandun J, Dill BD, Klinge S. Stage-specific assembly events of the 6-MDa small-subunit processome initiate eukaryotic ribosome biogenesis. Nat Struct Mol Biol. 2015;22(11):920-3.
46. Kos M, Tollervey D. Yeast pre-rRNA processing and modification occur cotranscriptionally. Mol Cell. 2010;37(6):809-20. PMCID: 2860240.
47. Maeder C, Kutach AK, Guthrie C. ATP-dependent unwinding of U4/U6 snRNAs by the Brr2 helicase requires the C terminus of Prp8. Nat Struct Mol Biol. 2009;16(1):42-8. PMCID: 2707180.
48. Mozaffari-Jovin S, Wandersleben T, Santos KF, Will CL, Luhrmann R, Wahl MC. Novel regulatory principles of the spliceosomal Brr2 RNA helicase and links to retinal disease in humans. RNA Biol. 2014;11(4):298-312. PMCID: 4075514.
49. Toseland CP, Martinez-Senac MM, Slatter AF, Webb MR. The ATPase cycle of PcrA helicase and its coupling to translocation on DNA. J Mol Biol. 2009;392(4):1020-32.
50. Arslan S, Khafizov R, Thomas CD, Chemla YR, Ha T. Protein structure. Engineering of a superhelicase through conformational control. Science. 2015;348(6232):344-7. PMCID: 4417355.
51. Ozgur S, Buchwald G, Falk S, Chakrabarti S, Prabu JR, Conti E. The conformational plasticity of eukaryotic RNA-dependent ATPases. FEBS J. 2015;282(5):850-63.